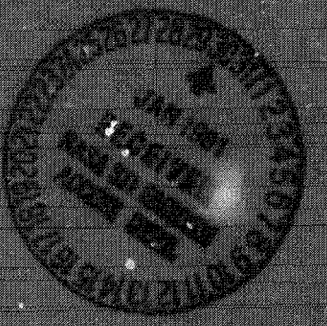

GAS TURBINE & PLASMA DYNAMICS LABORATORY
MASSACHUSETTS INSTITUTE OF TECHNOLOGY
CAMBRIDGE, MASSACHUSETTS

NSG-3187

An Experimental Study of the Effects of Swirl and Density Difference on Mixing in Shear Flows

C. S. Tan

GT & PDL Report No. 153 November 1980

Summary

Experiments have been carried out on the mixing of streams with and without swirl and with and without density differences in a coannular geometry. The flow process was visualized through the use of a phosphorescent tracer, 2-3 biacetyl. Three variations of the visualization techniques were used: direct excitation, collisional excitation and quenching of the tracer. Each technique is complementary to the others and yields information about turbulent transport, molecularly mixed and unmixed regions in the flow. The axial variation of the flow for the case with swirl in the inner annulus is investigated in some detail. From the flow visualization pictures, it is tentatively concluded that the initial Helmholtz instability of the tangential shear layer gives rise to small scale peripheral structures, then it is possible that the inner swirling stream drives an instability which turns these small scale peripheral structures into ones of larger scale, thereby rearranging the initial vorticity distribution of the flow field. The pictures also indicate the occurrence of interchange of fluid between the annuli. Relatively few data points were obtained for the co-flowing streams with density difference (nitrogen/helium or helium/nitrogen). During the course of the experimental work, an aspirating probe for concentration measurements was designed and built. From the flow visualization pictures, it is tentatively concluded that the interaction of density field with the resulting radial pressure gradient may have influenced the evolution of the flow structures.

Acknowledgement

The author would like to thank Professor J.L. Kerrebrock, and Professor W.K. Cheng (of the Mechanical Engineering Department at M.I.T.) for the helpful discussion and comments.

This research was sponsored by NASA Lewis Research Center under grant NSG-3187.

Table of Contents

I. Introduction

The mixing of two fluid streams, whether it be in confined or unconfined geometry, is of technical interest. A unique technique of flow visualization had been developed at the M.I.T. Gas Turbine Laboratory by S.C. Bates [1](1977), which makes it possible to examine the molecularly mixed layer between two gas streams. The technique also allows one to distinguish the mixed from the unmixed regions. S.C. Bates used the technique to study the mixing of a shear layer between two parallel streams.

W.K. Cheng[2] (1978) adopted the technique to study the effects of swirl on the mixing between two streams in a co-annular geometry. In the course of his investigation, he pointed out the existence of non-axisymmetric structures in an unstable swirling flow. An effort is made in the present investigation to visualize these structures in more detail for the case where only the inner stream of the co-flowing streams has swirl. To achieve this, the optical system was modified to allow better viewing, from the axial direction, of the peripheral structures discovered by W.K. Cheng[2]. A tunnel spacer was also added to enable the study of the flow field over a larger axial extent. An effort is also made to examine the effect of differences in density in such a flow system. During the course of the work, an aspirating probe was designed and developed for measurement of the relative concentration of a gas of different molecular weight in a background gas, for example of He in N_2, this being the gas combination employed to produce the density difference between the annuli. The development of this technique is in an early stage.

II. Flow Visualization Technique

The flow visualization technique used in the present experiment was developed by S.C. Bates[1] (1977) at the M.I.T. Gas Turbine Laboratory. Through the use of different modes of visualization (the direct excitation, the collisional excitation and the quenching modes), the technique can map out the molecularly mixed versus the turbulently mixed regions. For details of the technique, reference may be made to ref. (1). A brief description of the technique will be repeated here.

The fluorescent tracer used to visualize the flow is 2-3 biacetyl. It is a yellowish liquid at room temperature with a fairly high vapor pressure (40 mm). 2-3 biacetyl absorbs light from 3500 to 4600 Å, but fluoresces in the blue and phosphoresces in the green. The latter was used for the flow visualization here because it is 60 times brighter than the former. The quantum yield of the phosphorescence is about 15%.

In the direct excitation mode, one of the gas streams is seeded uniformly with biacetyl. The flow region of interest is illuminated by a thin sheet of light and the illuminated plane is photographed. Thus the image is a dissection of the flow at the illuminated plane. Note that unlike the shadograph and Schlerein methods, the image is not formed as a result of the integrated effect on the light along the line of sight, hence its adaptability for visualizing three dimensional structures. Under this mode of visualization, a picture of the mixing region depicts the spreading of the seeded stream into the unseeded one by both turbulent transport and molecular diffusion.

In the collisional excitation mode, one stream is seeded with biacetyl and the other with benzene. A thin sheet of UV light is passed through the flow region of interest. The UV light has no effect on biacetyl but optically pumps the benzene. The excited benzene molecules in turn cause the biacetyl to phosphoresce through molecular collisions by the transfer of optically induced molecular energy. Thus the recorded picture is a map of the molecularly mixed region in the flow.

In contrast, the quenching mode permits visualization of the molecularly unmixed region. The optical arrangement for this mode is the same as for the direct excitation. One of the streams is seeded with biacetyl while the other is seeded with oxygen. In the molecularly mixed region, the oxygen molecules quench the phosphorescence; thus, the recorded image shows the molecularly unmixed region of the stream containing biacetyl.

III. Experimental Apparatus

A. The tunnel and the gas flow system.

Figure 1 is a sketch of the tunnel and the gas flow system used in the present experiment. A detailed description of the tunnel is given in references (1) and (2). A brief description of the recent modifications is given here for continuity. There are two independent manifolds M1 and M2. One is fed by eight cylinders of helium, and the other by twelve cylinders of nitrogen. These gases enter pipes A and B via the sonic orifices. These sonic orifices regulate the flow rates and they are so adjusted that the axial velocity of either stream is about 7 ms^{-1} at the test section (thus the Reynolds number based on the annulus height is of the order of 10^4)[2]. Ball valves V1 through V4 allow the facility to be fed by gas of one type

only, or by gases of different types, in each pipe leading to the annulus tunnel, thus enabling the study of density effects.

Gases entering the tunnel are evenly distributed over the cross-section by choking orifices on plate C, then pass through screen D into a settling chamber. Contraction is provided to thin out the boundary layer before they enter the test section. The flows (swirling if turning vanes E and F are mounted) emerge to form a shear layer at the end of the splitting cylinder G. Since oxygen quenches the phosphorescence of the experiment, the whole apparatus must be capable of pumping down to about 100 microns of mercury. It is then filled with working gas before the start of the experiment.

The seed flow supplies from gas cylinders containing the organic liquids (biacetyl and benzene) diverts into the two branches. The inner annulus flow (A) is seeded with 2-3 biacetyl and the outer annulus flow (B) is not seeded for the direct excitation experiment, seeded with air for the quenching experiment, and with benzene for collisional excitation experiment. The cylinders are heated to deliver 2 to 3 mm of partial pressure of the seed vapour at the test section. The long pipes A and B, with a physical length to diameter ratio of about 120 ensure that the organic chemicals are uniformly mixed before entering the tunnel.

Because the tracer gas 2-3 biacetyl used in the experiment has a very unpleasant odor, the flow has to be discharged via a pneumatically controlled plexiglass door (also serves to keep air out) into a huge plastic baloon. A blower is then used to blow the tracer contaminated gas through an electric kiln (fig. 2) which has been heated to a temperature of about 2000°F.

so that the organic chemicals may be broken down before discharging into the building exhaust system. Five instrument ports are provided at the tunnel test section to allow the taking of hot-wire data and aspirating probe data. They are two inches apart with the first one 3 inches downstream from the splitting cylinder.

A test section spacer is provided so that the structure of the shear layer may be examined over a larger axial distance.

B. Input Output Optics

Details of the input and output systems are in references 1 and 2. A 200 joule capacitive flashlamp pulser drives an EG and G FX-38-C-3 Xenon flash tube to provide the input sheet of light. The light is collimated by a slit and two cylindrical quartz relay lenses into a thin sheet before entering the tunnel through a UV grade quartz window. A Pomfret Research Optics 2537 Å interference filter is used to obtain the UV light for the collisional experiment. The transmission efficiency of the filter is about 20% and the bandwidth is about 280°A. Figure 3 shows the optical arrangement.

The dim light emitted in the visualization experiment, after being collected by a Nikon f = 55mm/1:1.2 lens, passes through a green filter and falls on the input area of an ITT F 4747 microchannel image intensifier. Newly purchased, the gain of this device was 2×10^4. Over the years, with continuous use, its gain has deteriorated. The resulting ouput image of the flow region is recorded through contact photography with Polaroid type 57 film (ASA 3000). Pictures for direct excitation and quenching experiments are taken with exposure times of 750 μs at f/2.0, while those

for collisional mode are taken with exposure time of at least 1.5 ms at f/1.2.

C) Duration of the experiment.

The tunnel works in a blow down mode to conserve gas. The flow is initiated by a pneumatically actuated valve from a reservoir of gas cylinders. It lasted for about 2.5 sec. From the time history of the pressure tracer (Fig. 4) at the mixing pipes and tunnel, the flow is steady for at least 1.5 sec.

D) Hot wire measurements.

A triple hot-wire probe (DISA type 55-P91), operating in constant temperature mode, is used for measuring the three components of flow velocity at the test-section. Time resolved data, obtained by radially traversing the probe, or with the probe at a stationary point, are acquired over an axial distance of 18" (with the use of test section spacer). The duration of data acquisition is about 0.7 sec., during which the flow is steady. The data acquisition system is shown in fig. 5. The signal from the hot-wire is digitized using an MP 6912 analog-to-digital converter (with a capability of sampling at 100 KHz). A user built logic circuit then transfers the digital signals to the core memory of a DEC MINC 11/2 microcomputer, via a parallel input and output board on the microcomputer Q-bus. About 16,000 points of data are collected in each run. Thus a sampling frequency of 7 KHz is used for each hot-wire. After each run, the data are transferred from the core memory to a secondary storage (floppy diskettes) for permanent storage.

Previous documentation (including the computer program) of the use of this hot-wire probe was lost, therefore they had to be redeveloped for the present experiment. Some details for the use of this hot-wire probe are presented in Appendix A.

E. Aspirating probe measurement.

An aspirating probe has been designed to measure the relative concentrations of the constituents of binary mixture of gas. Details of the design of this probe and its operation are in Appendix B. The probe is estimated, using axisymmetric analysis, to have a spatial resolution of 0.65 mm and a frequency response of 25 KHz. When tested in a shock tube, the output signal had a rise time of 40 us, as shown in the Appendix. The probe was also tested in a stream of nitrogen of varying velocity for its response to changes in external velocity. This test indicated no changes in the output readings of the anemometer, verifying its design concept.

Some results are reported from this probe, but it must be considered in an early stage of development.

IV. Experimental data.

A. Introduction

In this section some experimental data are presented for the case where the inner annular stream has swirl, while the outer has none. The gas used for streams of equal density is nitrogen, while those for streams of different densities are nitrogen and helium. For each run, a flow visualization picture and a set of hot-wire probe traverse data/ or an aspirating probe traverse data can be obtained. Though efforts are made to ensure reproducibility in conditions for runs with the same nominal values,

variations in them may occur. Relatively few data points were obtained (24 pictures and 4 sets of raw data from the aspirating probes) for the co-flowing streams with different densities, all with the inner one swirling. In contrast to reference 2, flow visualization pictures of axial planes are taken with the camera mounted in such a way that it looks into the flow axially (see fig. 3b for the optical arrangement). It was hoped that this would enable better viewing of the peripheral structures of the flow-field. A tunnel spacer was added to the system to enable the viewing of the flow field over an axial distance of 14 in. Also it must be mentioned that, in contrast to the flow visualization data presented in references 1 and 2, only the direct excitation and quenching mode pictures are presented in details. The collisional excitation pictures obtained were of poor quality. At this stage, it is tentatively concluded that this is largely due to the deterioration of the gain of the ITT F4747 microchannel image intensifier through its usage over the years.

B. Hot-wire data.

Hot-wire traverse measurements were made at 10 axial stations. The stations are two inches apart (except 5 and 6, which are 1" apart), with the first one three inches downstream of the splitting cylinder. Fig. 6 shows the mean velocity components (radial, tangential and axial) plotted as functions of radius at axial stations 3", 5", 7", 9", 11" downstream of the splitting cylinder. These mean velocity components were obtained from 280 point averages (a simple moving average) over 5120 data points. Therefore these represent a time domain average of 4 ms and space domain average of 5 mm. It should be noted that the accuracy of the velocity components as

measured by the triple wire probe is subject to the limitations of the method used, as described in Appendix A. Furthermore, the triple wire probe is calibrated for speed and direction under static conditions but used for measurement of velocity components in highly turbulent flow.

No attempts are made to retrieve the fluctuating velocity components from the hot-wire data. We present some of the linearized signals from the triple wire probe in Fig. 7, for stations 1 to 10. These signals contain information about the flow structures. All the signals shown in Fig. 7 represent a full [illegible] ple-wire probe traverse outwards, starting at 1 cm from the centre body. At station 1, the signal has higher fluctuations in the inner annulus than in the outer annulus, where the signal is comparatively quiet. Note the discontinuity in the signal (in the neighbourhood of mid-annulus), at stations 1 and 2. This discontinuity indicates the position of the shear layer. The large fluctuations in the inner annulus seem to be spreading outwards progressively. At stations 9 and 10, the hot-wire signals seem to indicate that the flow is turbulent throughout the annulus. Careful perusal of the hot-wire data indicates that there is a definite sawtooth envelope superimposed on the fluctuating signal; this is especially well-defined at station 5. This probably indicates the presence of some recirculating eddies.

C. Data from aspirating probe.

Aspirating probe traverse measurements were made at axial stations 1 and 4 for two flow configurations, (i) where the inner annular flow was nitrogen and the outer annular flow was helium, and (ii) where the flow configuration in (i) was reversed. The plots in Figures 8 and 9 show the mean density profile for the four traverse measurements. The output

shown is the anemometer readings in volt, rather than in concentration. This is because the hot-wire element within the probe was broken while making the measurements; consequently, we are unable to check the calibration.

D) Flow visualization pictures.

Flow visualization pictures are presented for two cases:

(i) the co-flowing streams of equal density with the inner one set to swirl at a flow angle of 40 to 50°, (ii) the co-flowing streams of unequal densities with the inner one set to swirl at the same flow angle as in case (i). For case (ii), nitrogen is used in one stream while helium is used in the other. Some flow visualization data were obtained for the cases with the inner stream set to swirl, while the outer stream was set to swirl in the opposite direction and with the swirl in both streams, but they are not presented here. Pictures of the flow are taken on Polaroid type 57 film. The circular image is limited in area by the 18 mm diameter image intensifier output face (but they can be blown up). All the flow visualization pictures presented here are dissections of the flow field in a radial plane parallel to the axial direction or in an axial plane perpendicular to the axial direction. The center of the picture corresponds approximately to the middle of the annulus. For the pictures in a radial plane, the flow is from the right to the left.

The degree to which information can be retrieved depends very much on the quality of the flow visualization pictures. Reference may be made to (1) for discussion of this topic. The gain of the image-intensifier is spatially non-uniform, the image being considerably dimmer near the edges. This factor

should be taken into consideration while attempting to interpret the data. The collisional excitation pictures obtained are of poor quality; this is tentatively attributed to deterioration in the gain of the image intensifier unit.

Case (i):

In this case, both the inner and outer annular streams were of nitrogen. The inner stream was set to swirl at an angle of 45° to 50°. The axial velocity was about 7 to 8 ms^{-1}. Flow visualization pictures were taken over an axial extent of 14". No extensive or intensive efforts are made here to interpret each and everyone of the pictures obtained here, but features of the flow field that can be adduced from the pictures will be indicated.

The pictures numbering from 1 to 6 in fig. 10 are the direct excitation pictures of the flow field in the radial plane parallel to the axial direction. The number in inches by the side is the distance in inches the center of the picture is from the splitting cylinder. The letters a, b and c refer to flow visualization pictures taken at the same location with the flash tube fired at different times after the flow is steady for the blow-down period. This procedure is followed with the tacit assumptions that (i) the flow is repeatable from run to run with the experimental conditions kept constant (evidence may be provided by some of the flow visualization pictures). (ii) there may exist some structural eddies which are convected with the flow (note that the flow visualization picture represents a three inch circular flow field).

Pictures #1a and #1b have similar overall global features. The undulating interface may indicate the beginning of Helmholtz instability. However, pictures #2a to #2c, #3a to #3c, show some striking features. Picture #2a seems to indicate motion of fluid in the inner stream outwards (perhaps due to the centrifugal action of swirl, in accordance with Rayleigh's criterion),while pictures #2b, #2c, #3a and #3c, indicate the entrainment of lumps (very loose technical word) of fluid from the outer stream into the inner stream. What causes such transport of fluid elements and what role does such mechanism play in the mixing of the two streams? This could be due to: (i) the results of Hemholtz instability,or (ii) the results of the swirling flow which rearranges the vorticity present in the inner swirling flow into large scale motion, as seen in these pictures. Such features are not present in the flow visualization pictures for linear shear layers in references (1) and (2). Therefore it is tentatively concluded that the resulting instability (as given by Rayleigh criterion) may have resulted in the rearrangement of the vorticity originally in the inner swirling stream into such eddy motion. Another picture worth noting is number 5a. This picture indicates that some of the fluid elements have been pulled away entirely from the inner stream. Picture #5b indicates the fluid from the inner stream may have permeated the outer stream. Quenching pictures (fig. 11), indicate that at such a distance from the splitting cylinder, molecular mixing is rather complete among fluid elements from both streams. Pictures #1 to #5 in fig. 12 are the collisional excitation pictures. They show such poor definition that no attempt will be made to discuss them.

Pictures 1 to 15 in fig. 13 (direct excitation mode), show the dissection of the flow field in the axial plane at different distances from the splitting cylinder. Picture #1 shows a rather quiescent interface between the streams, while pictures 2 and 3 indicate some non-axisymmetric flow structures (some kind of small eddies) have begun to form. There could be a large number of such azimuthal structures around the peripheral. It is possible that the formation of such a large number of azimuthal modal structures may precede the development of large azimuthal modal structures, such as are evident in pictures 6, 7 and 10. Such large azimuthal modal structures are still present in pictures 11a, 12, 13, and 14b. It is of interest to note that some fluid elements from the outer stream have penetrated into the inner one near the centre body, as is evident in pictures 10 and 11 This could indicate an exchange of fluid elements between the two streams has occurred. Pictures 12, 13 and 14 are indicative of the fluid motion in pictures 2 and 3 of fig. 11. Pictures 14 and 15 indicate that fluid elements from the inner stream have permeated the outer stream and some fluid elements have actually parted from the inner stream. Pictures #1 to #10 in fig. 14 are the corresponding quenching pictures. Picture #10 of fig 14 and the collisional picture #1 of fig. 15 indicate that molecular mixing of eddies may have been quite thorough at 9-1/2" from splitting cylinder. From this set of pictures, we may tentatively conclude that the swirl in the inner stream (giving rise to instability, in accordance with Rayleigh's criterion) may have been responsible for the large scale motions in the neighborhood of the interface between the two streams, and in particular for the non-axisymmetric structures. The small scale peripheral

structures formed close to the splitting cylinder may be the result of Helmholtz instability of the tangential shear layer caused by swirl. The centrifugal action of the inner stream could then drive an instability, giving rise to larger peripheral structures.

Case (ii) -

Some preliminary flow visualization pictures have been obtained for the co-flowing streams of different densities (one helium and the other nitrogen) with the inner one set to swirl at 45° to 50°. The helium stream is set to have an axial velocity of about 8 to 9 ms^{-1} at the test section, while the nitrogen stream has an axial velocity of about 6 ms^{-1} at the test section. For this case, visualization pictures were taken only over an axial extent of 7". These are shown in figures 16 to 23. The pictures do indicate some qualitative differences in the flow features for the two configurations: (a) nitrogen in the inner stream and helium in the outer stream, (b) helium in the inner stream and nitrogen in the outer stream.

For the co-flowing streams of different densities with the inner one set to swirl, the following may play a part in the evolution of the flow field: (i) the swirl which sets up a pseudogravity field, (ii) the gravity effect set up by the unequal density interface (the strength of such effect, though small, varies circumferentially), and (iii) the difference in the fluid properties of the two streams (e.g., viscosity) which may influence the micro-structure of the flow field. The influence of (i) and (ii) may reinforce one another (e.g., at the lower half of the tunnel test section) or counteract against one another (e.g., in the upper half of the tunnel test section with nitrogen in the outer stream and helium in the inner stream.)

In the following, we will make an attempt to interpret the data for the two flow configurations, bearing in mind that there may be too few data points to come to any conclusive evidence of any particular flow features unique to such a flow system.

(a) with nitrogen in the inner stream and helium in the outer stream:

We have noticed that picture 1 of fig. 10 exhibits a continuous undulating feature (possibly indicating the inception of Helmholtz instability as mentioned), while such is not evident in picture 1 of fig. 16, except for the protruding fluid element into the outer stream.

It is possible that the density difference at the interface under the influence of a radial pressure gradient in the inner stream, could have accounted for the observed difference in flow features between the two. Local stability analysis of the shear layer with a radial pressure gradient in the inner stream shows that such a flow configuration would give rise to an enhanced Rayleigh-Taylor instability; this is indeed evident in pictures 2 and 3. In picture 3, the nitrogen has spread into the outer annulus while helium from the outer annulus has penetrated far into the inner annulus.

Fig. 17 shows the corresponding quenching pictures. Picture 3 shows an almost unmixed strand of fluid element lying across the annulus. Such a feature is not evident in all other quenching pictures obtained so far. What is seen <u>may be</u> a result of fluid motion driven by a density gradient in a pseudo-gravity field (i.e., the presence of a pressure gradient). The vorticity equation for an inviscid fluid with variable density is

$$\frac{\partial \underset{\sim}{\Omega}}{\partial t} + \underset{\sim}{V} \cdot \nabla \underset{\sim}{\Omega} = (\underset{\sim}{\Omega} \cdot \nabla) \underset{\sim}{V} + \frac{1}{\rho^2} (\nabla \rho \times \nabla p) \qquad (1)$$

where $\underset{\sim}{\Omega}$ is the vorticity, $\underset{\sim}{V}$ the velocity, ρ the density and p the pressure. This equation says that in the presence of pressure gradient (or acceleration field), vorticity is created in a fluid of variable density in motion. For such flows, vorticity, or rotation, is created so as to rotate the fluid until surfaces of constant density are normal to the pressure gradient (or acceleration vector field). Thus the resulting fluid motion might have rotated the fluid element from the inner annulus into the position shown in picture 3. It must be pointed out that the above explanation is arrived at through speculation on the mechanisms which influence evolution of fluid flow in streams of equal and different density and by process of elimination.

The pictures in figs. 18 and 19 are the direct excitation and quenching pictures taken for flow field in the axial planes. Pictures 1 and 2 in fig. 18 shows formation of small eddy-like azimuthal structures, while picture 3 (though overexposed) indicates the formation of a larger azimuthal structure. As for the quenching pictures, picture 3 shows that a considerable fraction of the fluid in the inner stream is molecularly mixed out (contrast with picture 4 of fig. 14 for homogeneous flow).

(b) with helium in the inner stream and nitrogen in the outer stream:

Picture 1 of fig. 20 indicates that the interface is not as quiescent as that in picture 1 of figs. 10 and 16. Further downstream, swirling instability (in the sense of Rayleigh's criterion) develops, thus enabling the spreading of the fluid from the inner stream to the outer stream as is evident in pictures 2 and 3 of fig. 20. The pictures in fig. 21 are the corresponding quenching ones. Notice the strand of almost unmixed fluid element from the inner stream lying across the annulus (though not as distinct as that in picture 3 of fig. 17). As in the case of configuration in ii, this

is likely to be due to the fluid motion driven by the density gradient in a combined gravity-acceleration field.)

The pictures in figure 22 and 23 are the direct excitation and quenching pictures of the flow field in the axial plane. They again indicate the development and presence of non-axisymmetric peripheral structures.

V. Some Concluding Remarks

Attempts were made to investigate the flow field of a co-flowing annular flow system over an axial distance of 14" through flow visualization pictures and hot-wire data. The inner annular stream had swirl, while the outer one did not. The effect of density difference on such a flow system is touched upon. An aspirating probe has been designed and built for concentration measurement, but no extensive use has been made of it for measurements yet; as only four traverse measurements of the concentration in binary gas flow system (helium/nitrogen) have been made. Interpreting the resulting data involves some extrapolation and speculation. It is tentatively concluded that:

(i) the initial Helmholtz instability of the shear layer gives rise to small scale peripheral structures; it is possible then that the inner swirling stream drives an instability (in the sense of Rayleigh's criterion), which turns these small scale peripheral structures into ones of larger scale, thus rearranging the initial vorticity distribution of the flow,

(ii) the hot-wire data indicates that the spread of turbulence into the outer annular stream is progressive rather than abrupt,

(iii) some of the hot-wire data have well defined envelopes, possibly indicating the presence of recirculating eddies.

It is also tentatively concluded that the density difference has an effect on the overall structure in such a flow system. Basing on the relatively few data points we have obtained so far, it is tentatively concluded that for the co-flowing steams of equal and unequal density in the present experimental set up, any qualitative difference in the flow features observed further downstream of the splitting cylinders is more likely caused

by the generation of vorticity due to the density gradient in the presence of a pseudo-gravity field (i.e., the radial pressure gradient).

VI. Suggestions for future work.

In the present set up for the optical system, one can only get a 2 to 3 inch circular view of the flow field. Based on such data, one then attempts to make a guess of the several flow structures. The optical arrangement should be modified to permit viewing of the larger flow field, especially a larger peripheral extent from the axial direction. This will aid in clarifying the flow structures.

More data have to be obtained for the co-flowing streams with unequal densities so that the effects of density difference can be elucidated. The aspirating probe can be used in conjunction with the triple wire probe to measure the velocity components.

There are many other parameters, such as those mentioned in reference 2; for instance, the Reynold number, which might affect the flow structures. They have yet to be investigated.

It is noted that the annular flow system is of simple geometry and thus it makes the spectral method (i.e., pseudospectral, Tau or Galerkin Approximations) attractive for numerically simulating the flow structures in such a system. Such method for studying the basic fluid phenomena in such a flow system may be considered in conjunction with future experimental work.

Lastly, future efforts should also be directed in an attempt to quantify the experimental data.

Appendix A

The Triple Hot-wire Probe Operation

(a) Introduction

The use of the DISA type 55-P91 triple hot-wire probe goes along the same line as described in Appendix A of reference (2) with minor difference in the method of retrieving velocity components. However, the computer program developed in reference (2) for fitting calibration data to models representing the operation of the triple probe and those for retrieving the three components of velocity from the hot-wire readings cannot be traced, consequently new computer programs for the purposes have to be re-developed for the present experiments. The probe is operated in constant temperature mode using the three identical anemometers described in A2 of Appendix A in reference (2). In using this probe, it is assumed that the dependence of speed and geometry of the triple wire probe can be neglected; otherwise its use would involve a thorough calibration of the probe at all possible orientations and within speed range of interest at each orientation. This assumption also permits the user to do the speed calibration and directional calibration separately.

(b) Calibration

The calibration (both speed and directional) of the triple wire probe was done in the low turbulence wind tunnel of the M.I.T. Aero & Astro Department. The MINC 11/2 microcomputer was used for the purpose. The readings from the triple hot-wire and that of pressure transducer (dynamic

head of wind tunnel section) were digitized using the Datel ST-LSI-2 analog-to-digital converter. At the end of calibration, they were transferred to floppy diskettes for permanent storage.

(1) Speed Calibration

Each wire in the probe is calibrated against the speed in the wind tunnel by orientating the probe such that the output reading from the anemometer is the maximum [2]. This ensures that the wind direction is perpendicular to the wire. The wire is calibrated in air but the result is rescaled for use in nitrogen[2] using King's Law:

$$Nu = A + B\,R_e^n \qquad (A.1)$$

or

$$\frac{E^2}{K\Delta T} = A + B\left(\frac{\rho}{\mu}u\right)^n \qquad (A.2)$$

where Nu = Nusselt No

Re - Reynold No

E = Output voltage from anemometer

K = thermal conductivity of gas

ρ = density of gas

μ = viscosity of gas

} at the mean temperature of the wire and the ambient

The constant A and B are found from the calibration data using linear regression analysis.

Each wire was calibrated for speeds ranging from 0 to 15 ms^{-1}.

(ii) Directional Calibration

Let Z_i be the effective wind speed as seen by wire i (i = 1 to 3) and $\underline{u} = (u_1, u_2, u_3)$, where u_i are the velocity components in a suitable laboratory co-ordinates system, then the effective velocities Z_i are related to $\underline{u}$ through

$$[\underset{\sim}{Z}] = [\underset{\sim}{A}][\underset{\sim}{Q}] + [\underset{\sim}{C}] \tag{A.3}$$

where $\underset{\sim}{Z} = \begin{bmatrix} Z_1^2 \\ Z_2^2 \\ Z_3^2 \end{bmatrix}$ and $Q = \begin{bmatrix} u_1^2 \\ u_2^2 \\ u_3^2 \\ u_1u_2 \\ u_2u_3 \\ u_3u_1 \end{bmatrix}$

The $\underset{\sim}{A}$ and $\underline{C}$ are the calibration constants given by

$$\underset{\sim}{A} = \begin{bmatrix} A_{11} & A_{12} & A_{13} & A_{14} & A_{15} & A_{16} \\ A_{21} & A_{22} & A_{23} & A_{24} & A_{25} & A_{26} \\ A_{31} & A_{32} & A_{33} & A_{34} & A_{35} & A_{36} \end{bmatrix} \quad \text{and} \quad \underset{\sim}{C} = \begin{bmatrix} C_1 \\ C_2 \\ C_3 \end{bmatrix}$$

Thus altogether there are twenty-one calibration constants. They are found by fitting the model to the m calibration data points using multiple linear regression analysis, which yields a matrix equation. They can be inverted to yield $\underset{\sim}{A}$ and $\underset{\sim}{C}$, i.e.,

$$\left[\alpha_i \right] = \left[\left[\underset{\sim}{X} \right]^T \left[X \right] \right]^{-1} \left[X \right]^T \left[\beta_i \right] \tag{A.4}$$

where

$$\left[\alpha_i \right] = \left[A_{i_1} \quad A_{i_2} \quad A_{i_3} \quad A_{i_4} \quad A_{i_5} \quad A_{i_6} \quad C_i \right]$$

$$\left[\beta_i \right] = \left[(\bar{z}_i^2)_1 \; . \; . \; . \; (\bar{z}_i^2)_j \; . \; . \; . \; (\bar{z}_i^2)_m \right]$$

and

$$\left[X \right] = \begin{bmatrix} (u_1^2)_1 & (u_2^2)_1 & (u_3^2)_1 & (u_1u_2)_1 & (u_2u_3)_1 & (u_3u_1)_1 & 1 \\ \vdots & & & & & & \\ (u_1^2)_j & (u_2^2)_j & (u_3^2)_j & (u_1u_2)_j & (u_2u_3)_j & (u_3u_1)_j & 1 \\ \vdots & & & & & & \\ (u_1^2)_m & (u_2^2)_m & (u_3^2)_m & (u_1u_2)_m & (u_2u_3)_m & (u_3u_1)_m & 1 \end{bmatrix}$$

where i runs from 1 to 3

and j denotes the j^{th} calibration points

The directional calibration is done by orientating the probe for a few sets of speeds. A typical example would involve rolling the triple-wire probe through 240° for 3 sets of yaw angles and 2 to 3 sets of speeds (in the range of interest), thus m can run from 126 to 225.

(iii) Retrieving the velocity components:

The equations (A.3) relating the effective velocities as seen by the triple wire probe to the velocity components in the laboratory co-ordinates form a set of non-linear algebraic equations. Given the three values of effective wind speeds (as determined from the triple hot-wire probe readings), we have to solve the set of non-linear algebraic equations for the three-components of velocity in laboratory co-ordinates system. It is the author's experience that sometimes as many as eight sets of roots may be obtainable. Thus, the flow direction has to be partially known for retrieving the velocity components from the knowledge of effective wind speeds. Here, we use the Levenberg/Marquardt iteration method (modification of classical Newton-Raphson iteration) to look for the three components of velocity from eqn. (A.3) (in contrast to the first-order gradient search method in reference 2).

The method goes as follows:

We replace $\underset{\sim}{u}^{(k)}$ estimate of $\underline{u}$ by

$$\underset{\sim}{u}^{(k+1)} = \underset{\sim}{u}^{(k)} + \Delta\underset{\sim}{u}^{(k)} \tag{A.5}$$

where $\Delta\underset{\sim}{u}^{(k)}$ is the solution of the system of linear equations

$$\sum_{j=1}^{3} \{\gamma^{(k)} I_{ij} + \sum_{t=1}^{3} J_{ti}^{(k)} J_{tj}^{(k)}\} \Delta u_j^{(k)} = - \sum_{t=1}^{3} J_{ti}^{(k)} f_t(\underset{\sim}{u}^{(k)}) , \tag{A.6}$$

where k is the iteration index, $\underset{\sim}{I}$ is the identity matrix and $\underset{\sim}{J}$ is the Jacobian.

$$\underset{\sim}{f}(\underset{\sim}{u}) = [\underset{\sim}{A}]\,[\underset{\sim}{Q}] + [\underset{\sim}{C}] - [\underset{\sim}{Z}]$$

$$J_{ij}^{(k)} = \left[\frac{\partial f_i}{\partial x_j}\right]_{\underset{\sim}{u}=\underset{\sim}{u}(k)}$$

The Jacobian $J_{ij}^{(k)}$ can either be evaluated numerically or analytically. $\gamma^{(k)}$ is a positive parameter which is being calculated so that

$$\sum_{i=1}^{3}\left[f_i(\underset{\sim}{u}^{k+1})\right]^2 < \sum_{i=1}^{3}\left[f_i(\underset{\sim}{u}^{(k)})\right]^2$$

(iv) Some remarks on the use of triple hot-wire proble:

Some results of the directional calibration of the probe are shown in figures (A.1) to A.4). As pointed out in Appendix A of reference (2), the model equation (A.3) does give negative values of Z_i^2 and has been forced to zero in the figures. Also there are regions where the calibration curves are co-linear, which may cause an uncertainty in the determination of the velocity components.[2]

Solutions $\underset{\sim}{u}$ to equation (A.3) are non-unique. It seems that to use this triple probe for measuring the fluctuating components of velocity, one may have to resort to a thorough calibration of the probe. The probe also suffers from drift in cold resistance and thus it has to be calibrated every time before use,[2] a time consuming process.

It must also be mentioned that in using the Levenberg/Marquardt iteration scheme, the method may converge to a stationary point which is not a solution.

Appendix B

Aspirating Probe

(i) Introduction

An aspirating probe was designed and built with the aim of measuring gas concentrations in co-flowing streams of differing density. In what follows, a brief description of the operating principle and its design is given.

(ii) Operating Principle

Basically, the probe (Fig. B.1) consists of a hot-wire sensing element (tungsten is used here) placed in a cylindrical duct of constant area followed by a throat. The throat exits into a chamber being pumped to vacuum, so that with the probe placed in a stream, the flow is choked at all times. The hot-wire sensing element is connected by leads to an anemometer (DISA 55D01) operating in a constant temperature mode. The mass flow rate is given by

$$(\rho U)_s = \sqrt{\frac{\gamma}{R}} \frac{Pt}{\sqrt{T_t}} \left[\left(\frac{2}{\gamma+1}\right)^{\frac{(\gamma+1)}{2(\gamma-1)}} \right]$$

where ρ is the density

U is the velocity

P is the pressure

T is the temperature

γ is the specific heats ratio

R is the gas constant $\left(= \frac{\text{universal gas constant}}{\text{molecular weight}} = \frac{Ro}{M_w} \right)$

and subscripts t and s refer to stagnation values and sonic values.

Thus for a given gas mixture, the maximum flow rate per unit area is dependent upon $P_t/\sqrt{T_t}$ only, if the stagnation conditions are held constants, then for a given gas, the Mach number M is fixed for a fixed geometry; (i.e.,fixed area ratio,

$$A/A_s = \frac{1}{M}\left[\frac{2}{\gamma+1}\left(1 + \frac{\gamma-1}{2} M^2\right)\right]^{\frac{(\gamma+1)}{2(\gamma-1)}} .$$

Using the basic gas dynamic relations, it can be deduced that ρ, P, T and U are constants, so that the hot-wire element responds only to gas concentration and stagnation conditions. For a binary mixture of gases, at the same T_t, the P_t can change due to the viscosity of gases (especially at solid surfaces, or mixing). But the fractional change in P_t can at most be $O(M^2)$. Thus for low speed flow, such a probe may only respond to gas concentration.

In the next section, we will indicate how one can estimate the response time of the probe.

(iii) Estimation of Response Time

In this analysis, it will be assumed that

(a) the lateral velocity v is much smaller than the longitudinal velocity U (i.e., $\frac{v}{U} << 1$)

(b) the flow is incompressible up to the probe intake

(c) the flow is inviscid

The method of singularities (sinks, sources and ring vortices) allows the flow past this probe to be calculated. Instead of using distribution of ring vorticies (a more elaborate and complicated way involving the manipulation of various types of integral), we use a much simpler approach here.

The probe may be approximated by a half-Rankine axisymmetric body. The sampling action of the probe may be simulated by a sink placed at the tip of the probe (See fig. B.2). If the sampling rate of the probe is much smaller than $U_\infty D_\infty^2$, then the Rankine axisymmetric body will not be altered significantly. With these in mind, and with reference to fig.B.2, the stream function for the flow is given by

$$X = \frac{1}{2} r^2 U_\infty + U_\infty \frac{d_T^2}{8} \frac{X}{\sqrt{x^2+r^2}} - U_\infty a^2 \frac{(x-a)}{\sqrt{r^2 + (x-a)^2}} \qquad (B.2a)$$

where d_T is the diameter of the capture streamtube, and $a = \frac{1}{4} D_\infty$, with D_∞ as the diameter of the unperturbed Rankine-type axisymmetric body. In dimensionless form (based on D_∞ and U_∞), the streamlines are given by

$$\frac{1}{2} r^2 - \frac{(x-\frac{1}{4})}{16\sqrt{r^2 + (x-\frac{1}{4})^2}} + \frac{d_T^2}{8} \frac{X}{\sqrt{x^2 + r^2}} = \text{constant} \qquad (B.3)$$

while the stagnation points are given by (r,x) which satisfies

$$1 + \frac{(X - \frac{1}{4})}{16\left[r^2 + (x-\frac{1}{4})^2\right]^{3/2}} - \frac{d_T^2}{8} \frac{X}{(X^2 + r^2)^{3/2}} = 0 , \qquad (B.4)$$

and

$$\frac{r}{16\left[r^2 + (X - \frac{1}{4})^2\right]^{3/2}} - \frac{d_T^2}{8} \frac{r}{(X^2 + r^2)^{3/2}} = 0 \qquad (B.5)$$

simultaneously.

The above axisymmetric analysis would give a flow field as shown in fig. B.3. For the dimension of the probe shown in fig. B.1, the lateral spatial resolution of the sampling volume would be about 0.7 mm. The longitudinal spatial resolution of the sampling volume is determined by the frequency response of the probe (e.g., for a flow speed of 7 ms^{-1} with a probe response of 25 KHz, the resolution would be about 0.30 mm). Fig. B.4 shows the variation of time τ taken by the fluid element in the sampling volume to reach the probe with the streamlines within the capture stream tube. Of course, it would take the fluid element on the stagnation streamlines an infinite amount of time to reach the probe. Thus, an estimate of the response time τ would be given by

$$\tau^* = \frac{\int_{\psi_0}^{\psi} t\,d\psi}{\int_{\psi_0}^{\psi} d\psi} \qquad (B.6)$$

For the given built probe shown in fig. B.1 and Fig. B.5, the response time was estimated to be about 40 μs. The given probe was tested in the M.I.T. Gas Turbine Laboratory shock tube, as shown in Fig. B.6. The rise time was measured (using Nicolet Explorer Digital Oscilloscope Model 206) to be about 40 μs (Fig. B.7a and B.7b).

It is noted that the sensing element is placed at a position in the duct where the flow (laminar) is expected to be fully-developed.

References

1. Bates, S.C., "Luminescent Visualization of Molecular and Turbulent Transport in a Plane Shear Layer," GTL Report No. 134, June 1977.

2. Cheng, W.K., "Turbulent Mixing in Swirling Flow," GTL Report No. 143, September 1978.

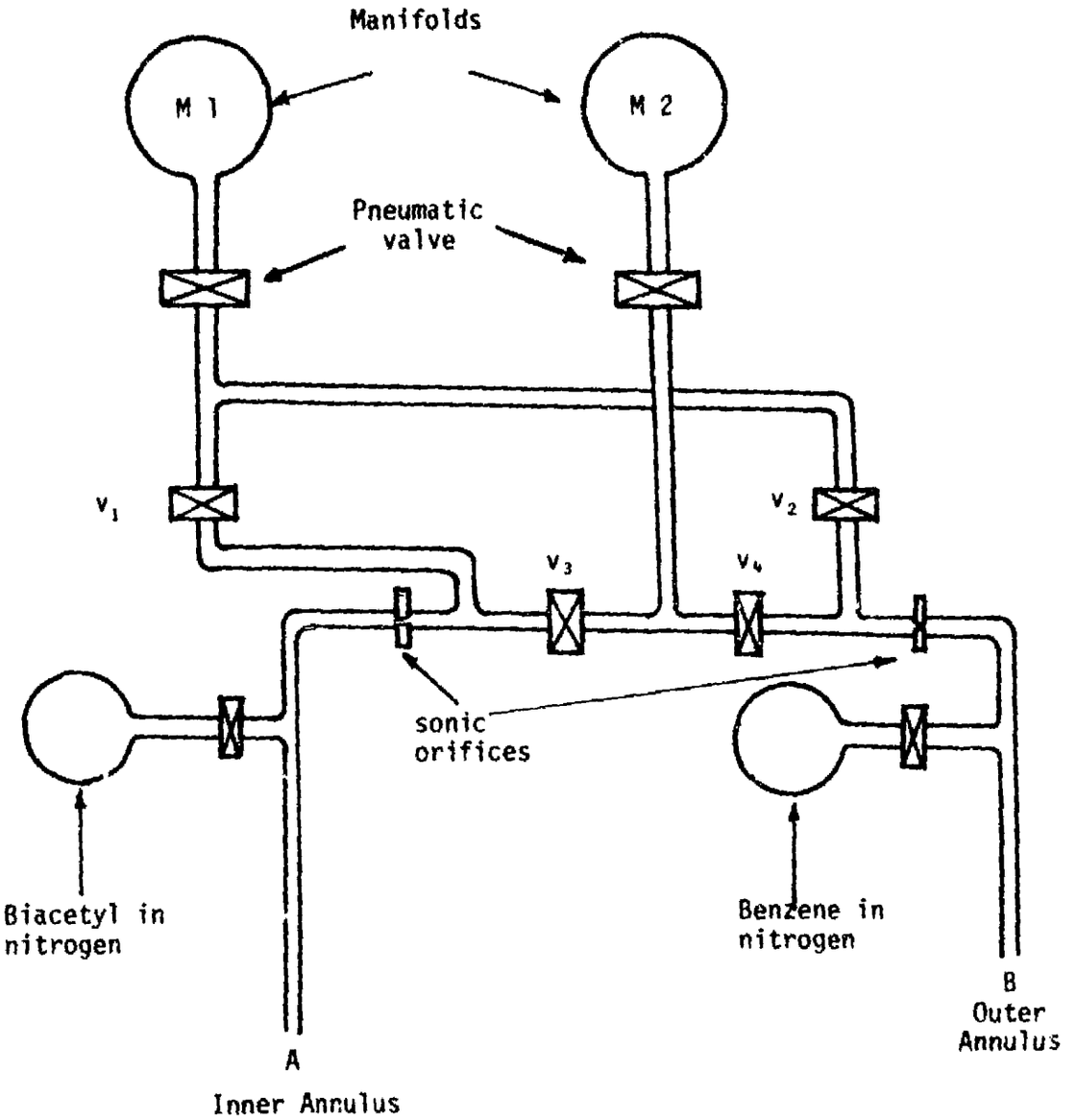

Fig. 1a Flow System

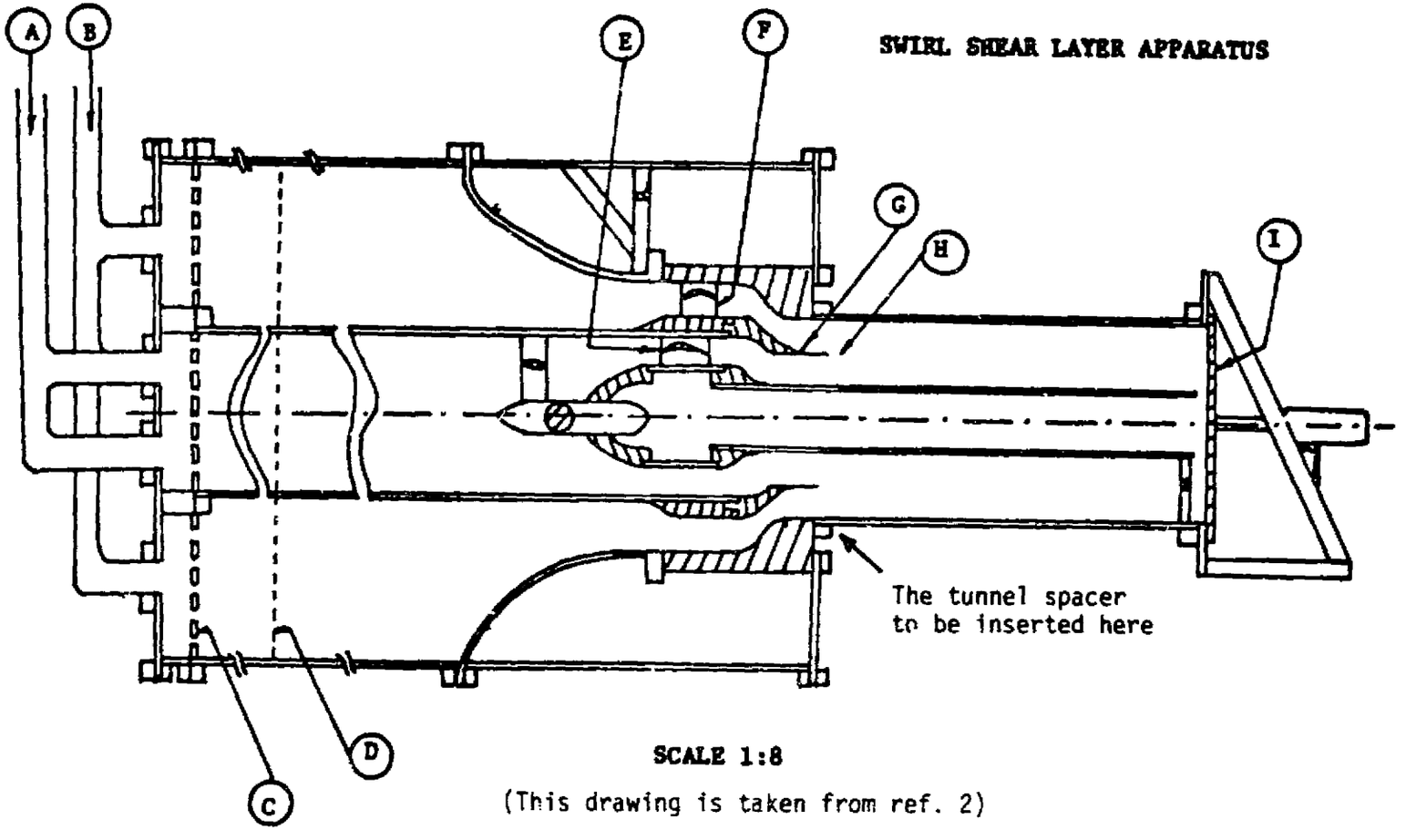

SCALE 1:8

(This drawing is taken from ref. 2)

Fig. 1b

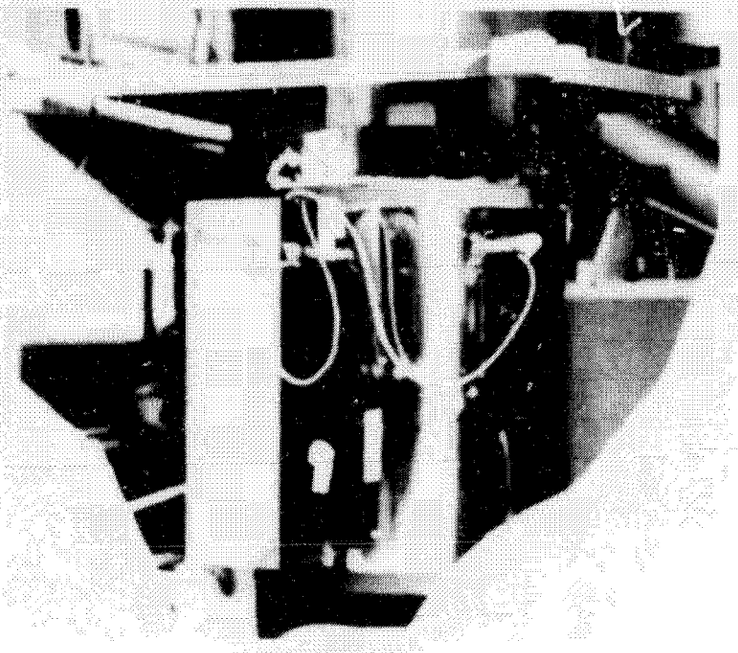

Fig. 2: Electric kiln used to break down the organic chemicals before dumping into the laboratory exhaust system.

OPTICS ARRANGEMENT - ILLUMINATED PLANE PARALLEL TO TUNNEL AXIS

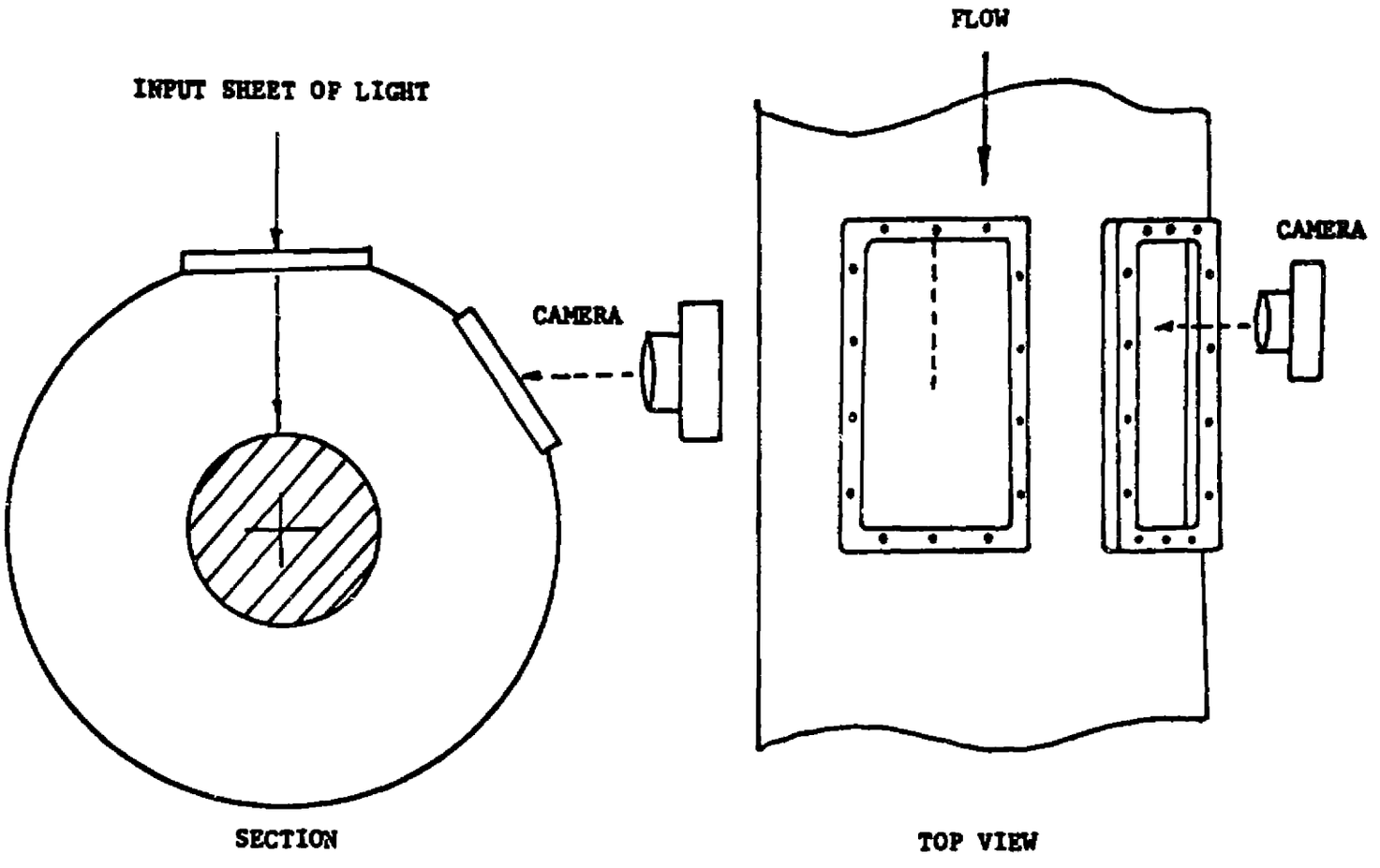

(This is taken from ref. 2)

Fig. 3a

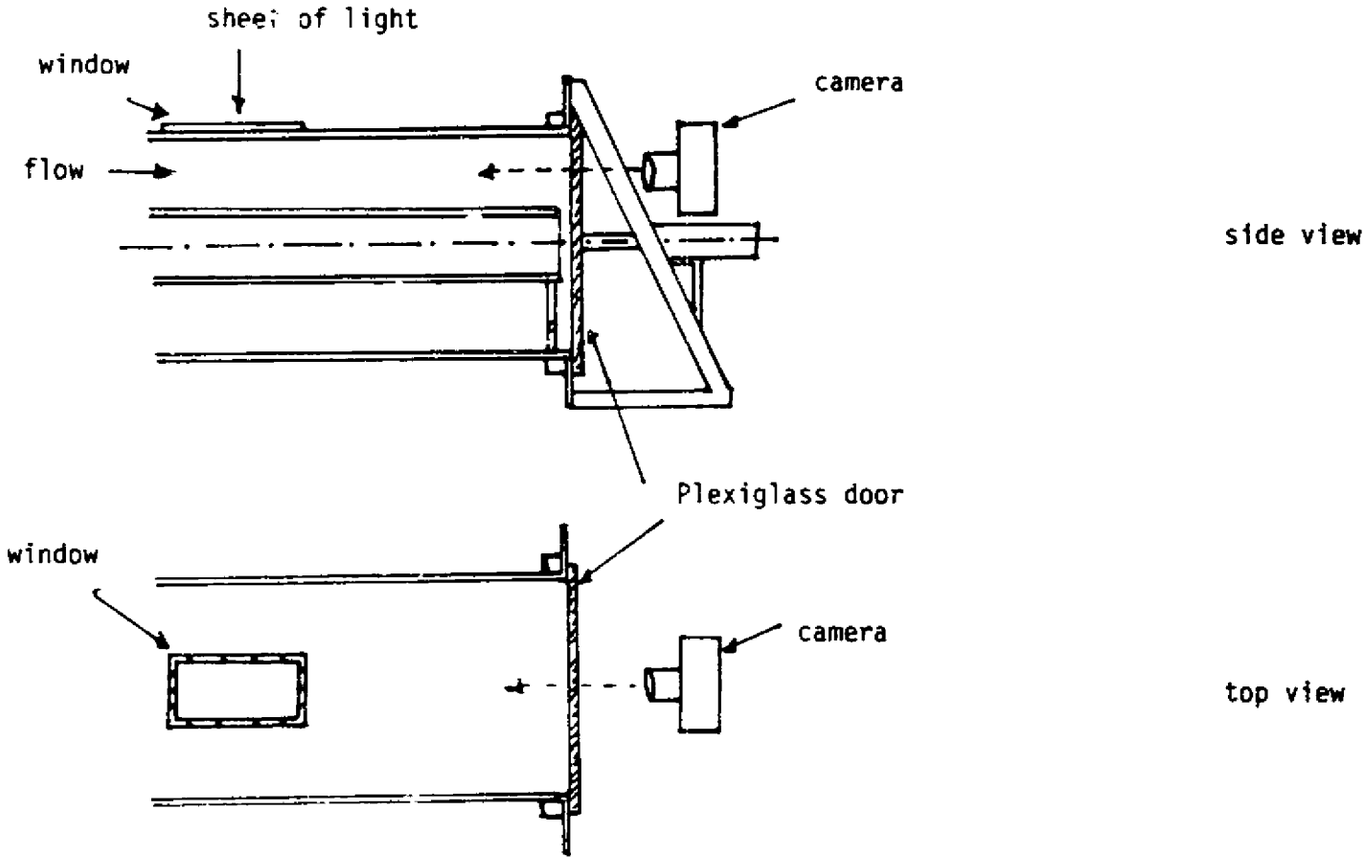

Fig. 3b Optics arrangement for viewing flow plane perpendicular to axis

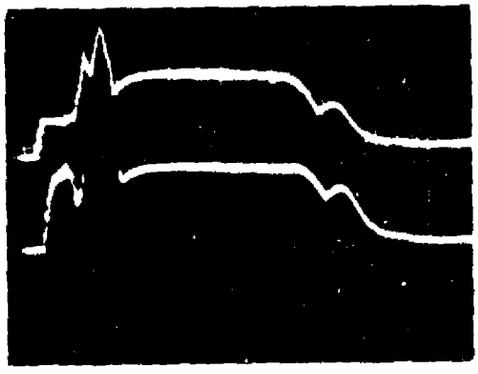

Upper beam: at mixing pipe of inner annulus

Scale: Horizontal = 0.5 sec/cm
Vertical = 0.2v/cm
(10 psig/cm)

Lower beam: at test section

Scale: Horizontal = 0.5 sec/cm
Vertical = 0.05v/cm
(0.5 psid/v)

Fig. 4a: Flow-time history (with no tunnel spacer added on)

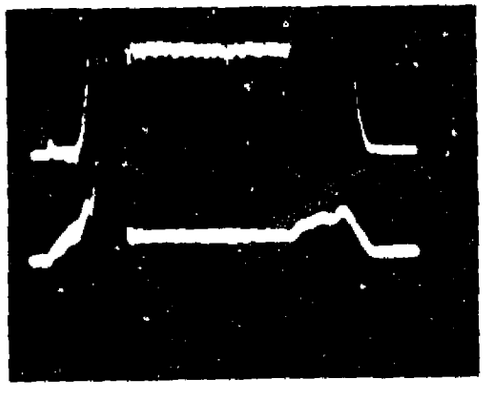

Upper beam: at mixing pipe of outer annulus

Scale: Horizontal = 0.5 sec/cm
Vertical = 0.05v/cm
(2.5psig/cm)

Lower beam: at test section

Scale: Horizontal = 0.5 sec/cm
Vertical = 0.05v/cm
(0.05psid/cm)

Fig. 4b: Flow-time history with tunnel spacer added on.

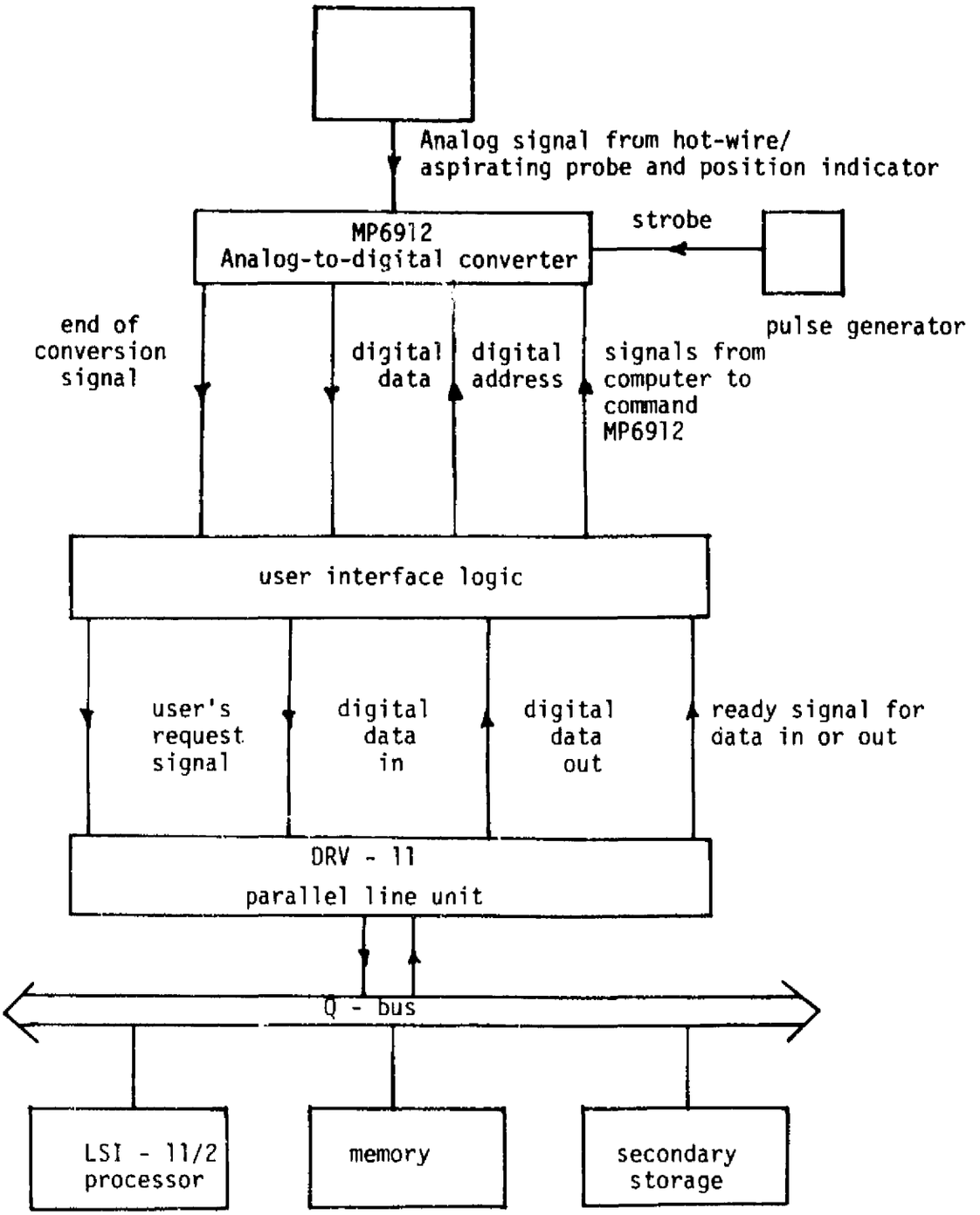

DEC MIINC 11/2 microcomputer

Fig. 5 Data acquisition system

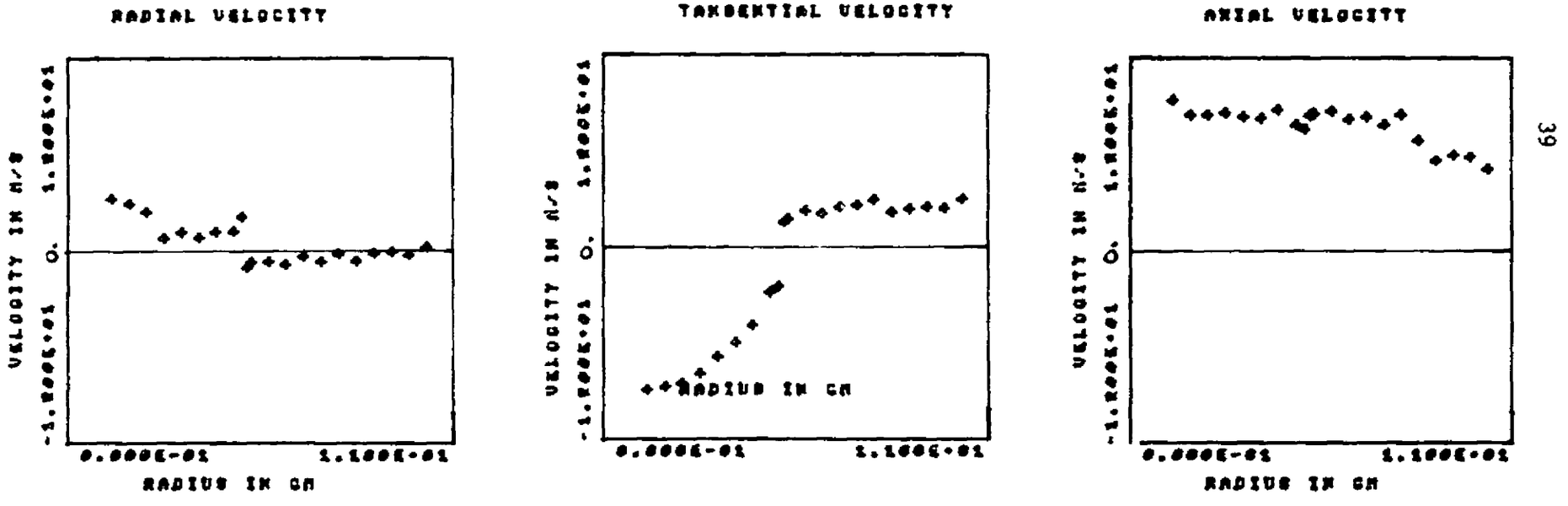

Fig. 6a Mean velocity components at station 1

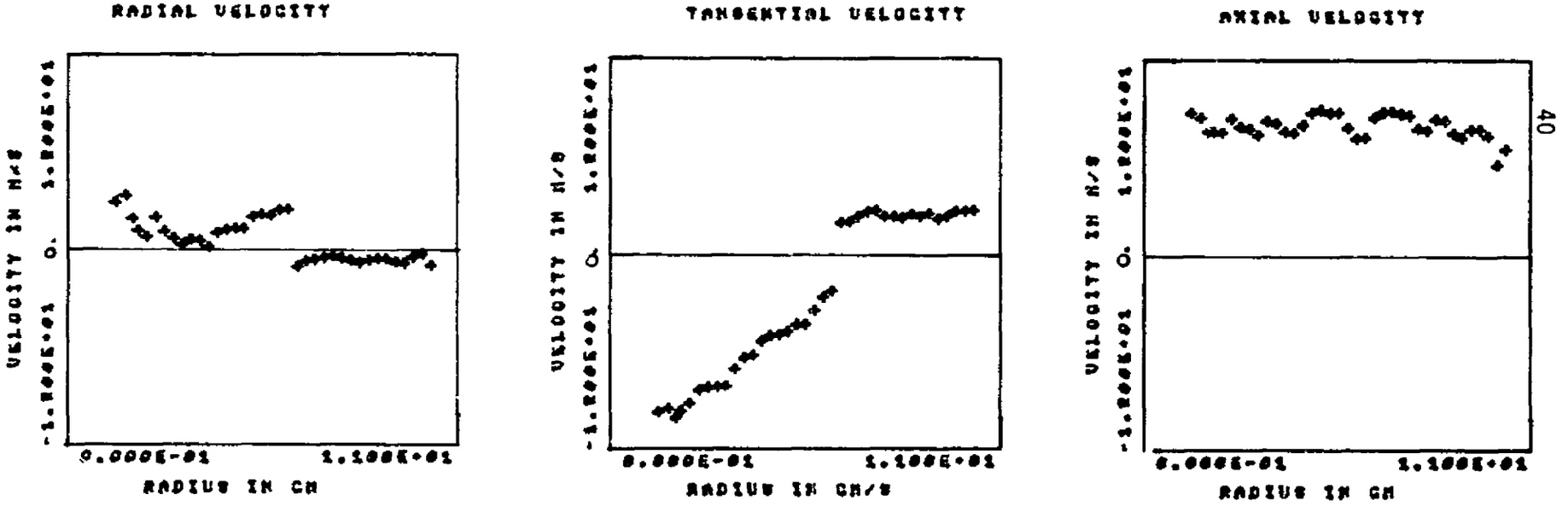

Fig. 6b Mean velocity components at station 2

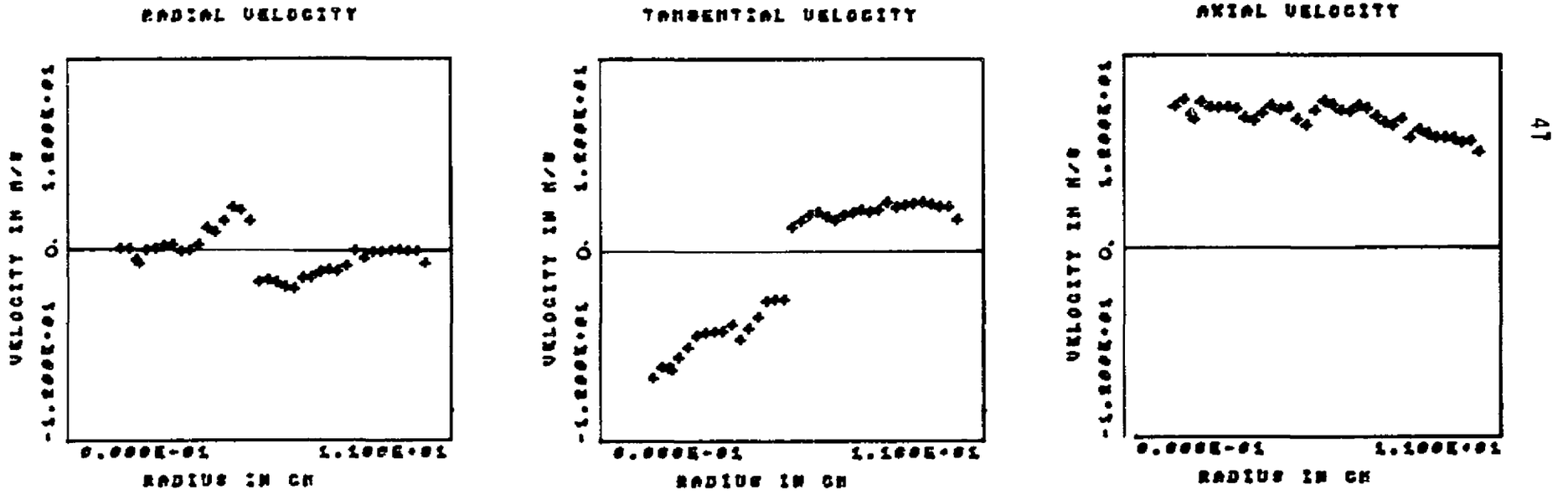

Fig. 6c Mean velocity components at station 3

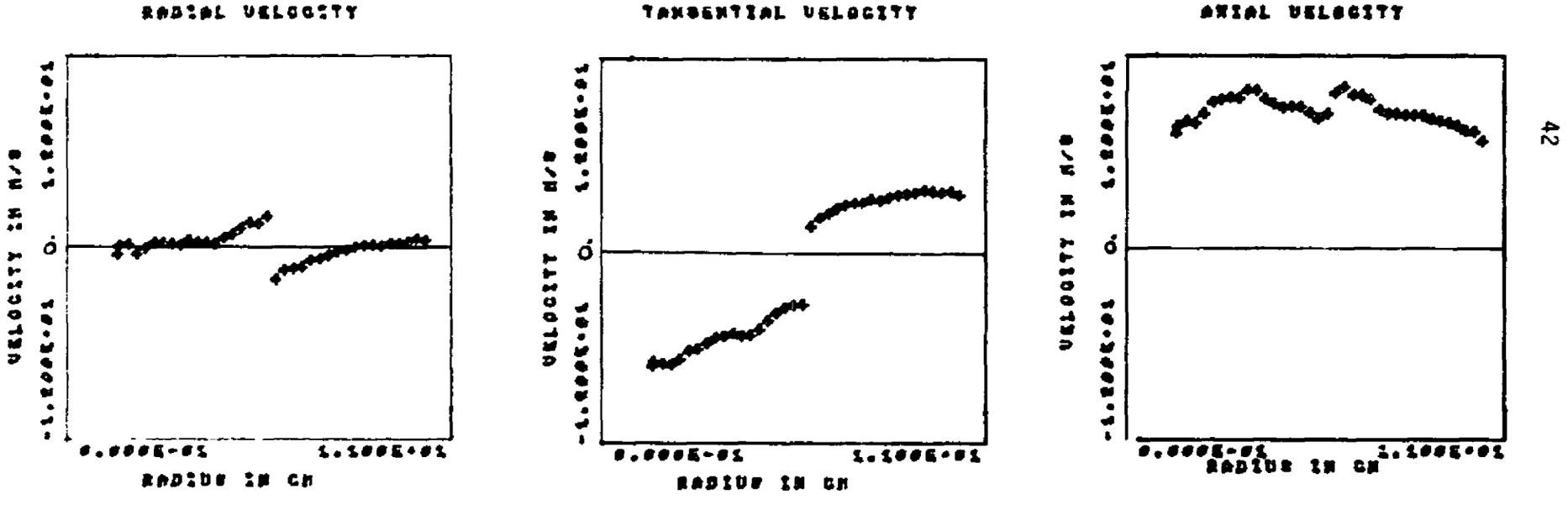

Fig. 6d Mean velocity components at station 4

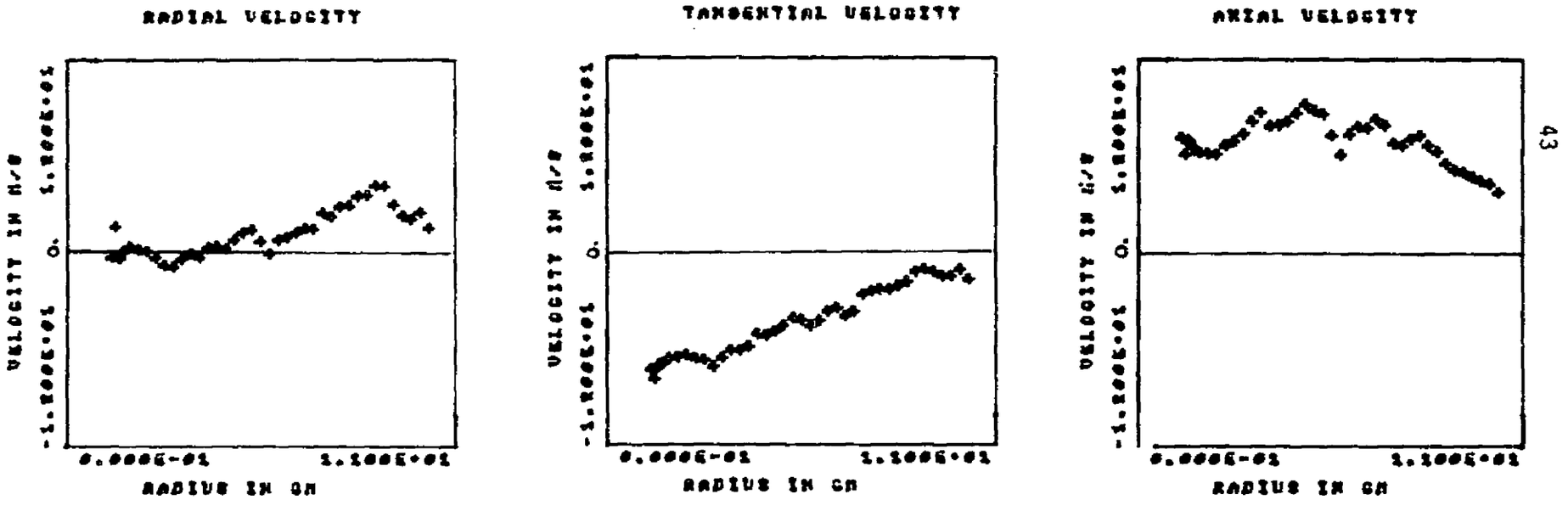

Fig. 6e Mean velocity components at station 5

Fig. 7: Linearised signal from the triple-wire probe at station 1 through station 10

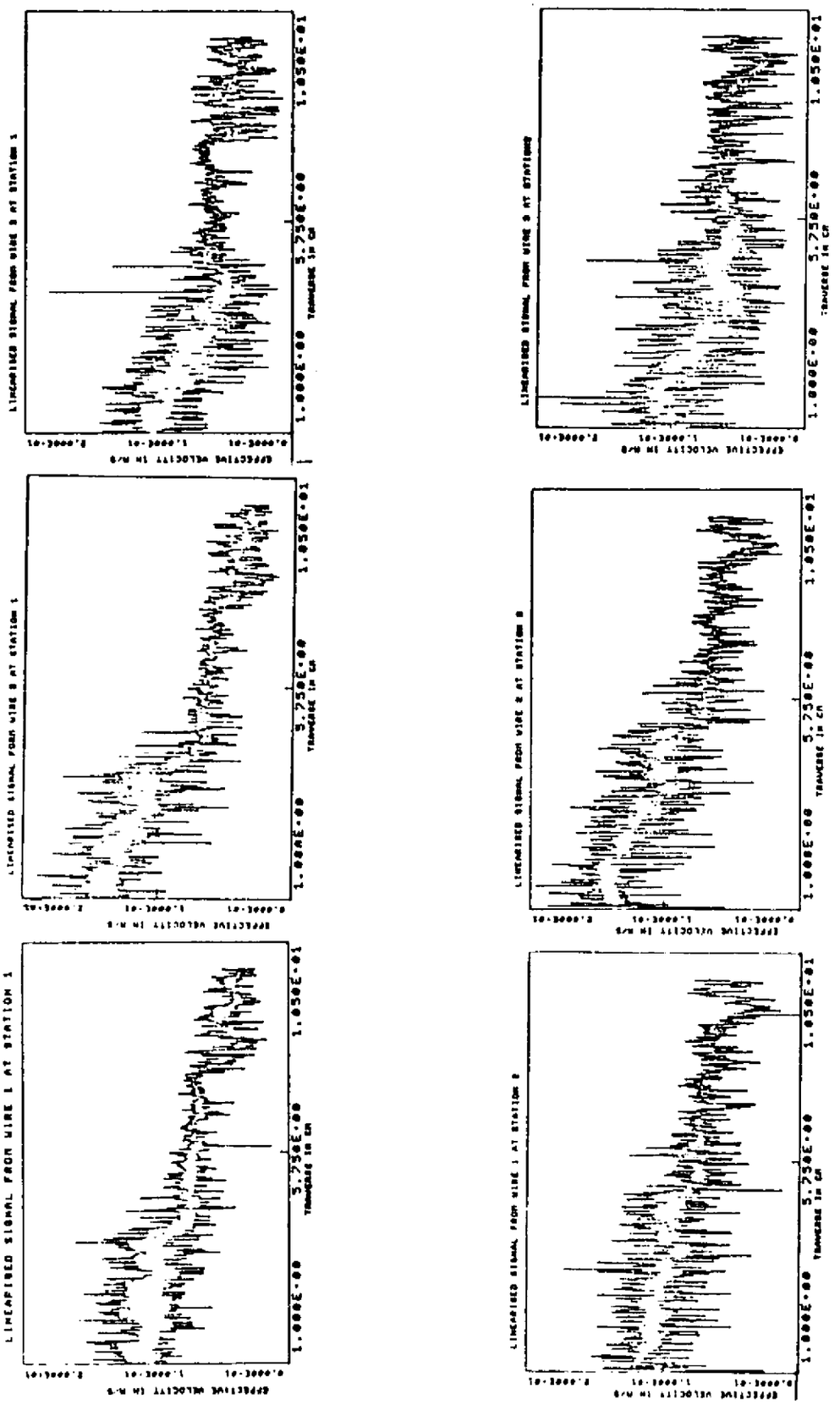
LINEARISED SIGNAL FROM WIRE 1 AT STATION 1
LINEARISED SIGNAL FROM WIRE 2 AT STATION 1
LINEARISED SIGNAL FROM WIRE 3 AT STATION 1
LINEARISED SIGNAL FROM WIRE 1 AT STATION 2
LINEARISED SIGNAL FROM WIRE 2 AT STATION 2
LINEARISED SIGNAL FROM WIRE 3 AT STATION 2
EFFECTIVE VELOCITY IN M/S
TRANSVERSE IN CM
1.000E-00
5.750E-00
1.050E-01

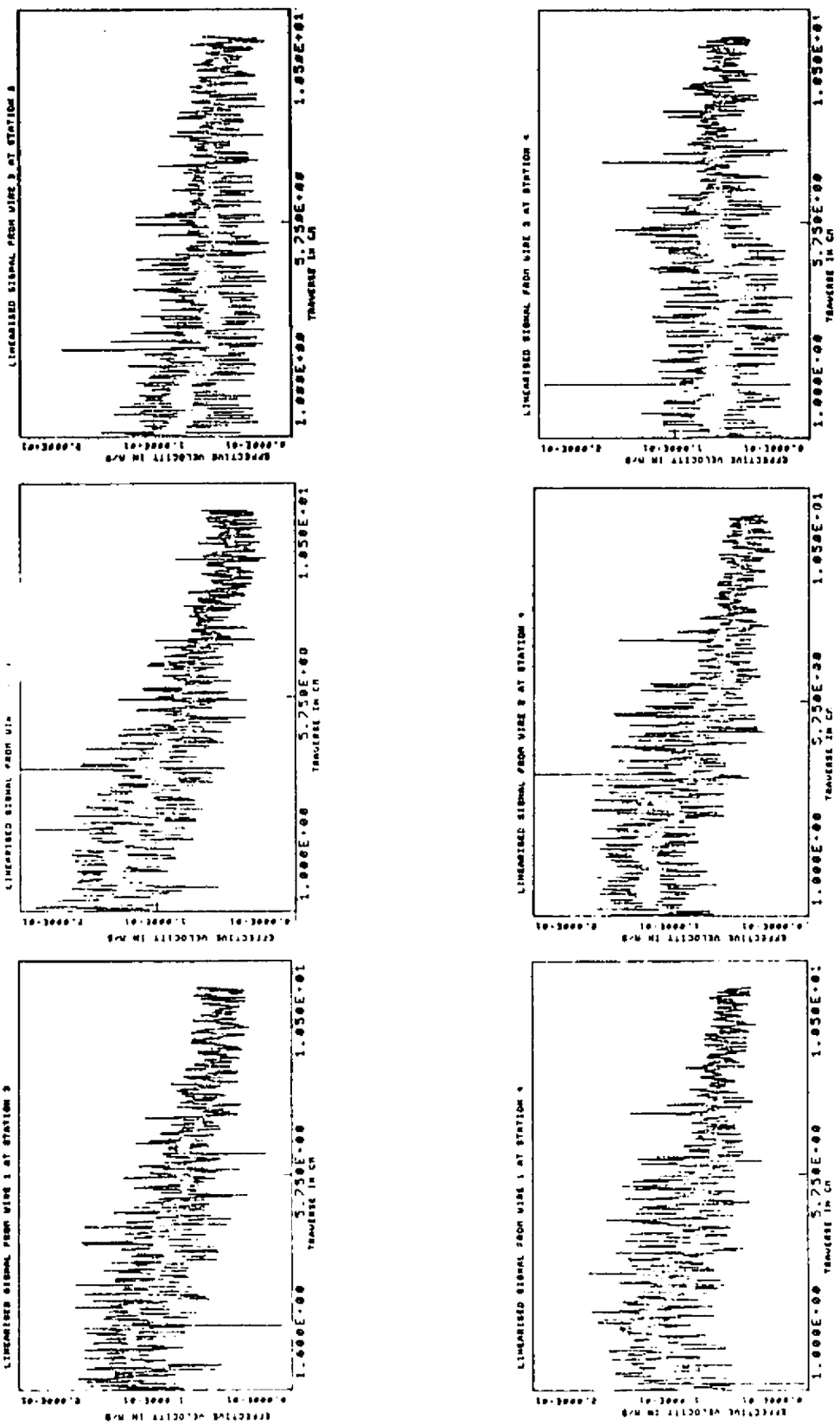

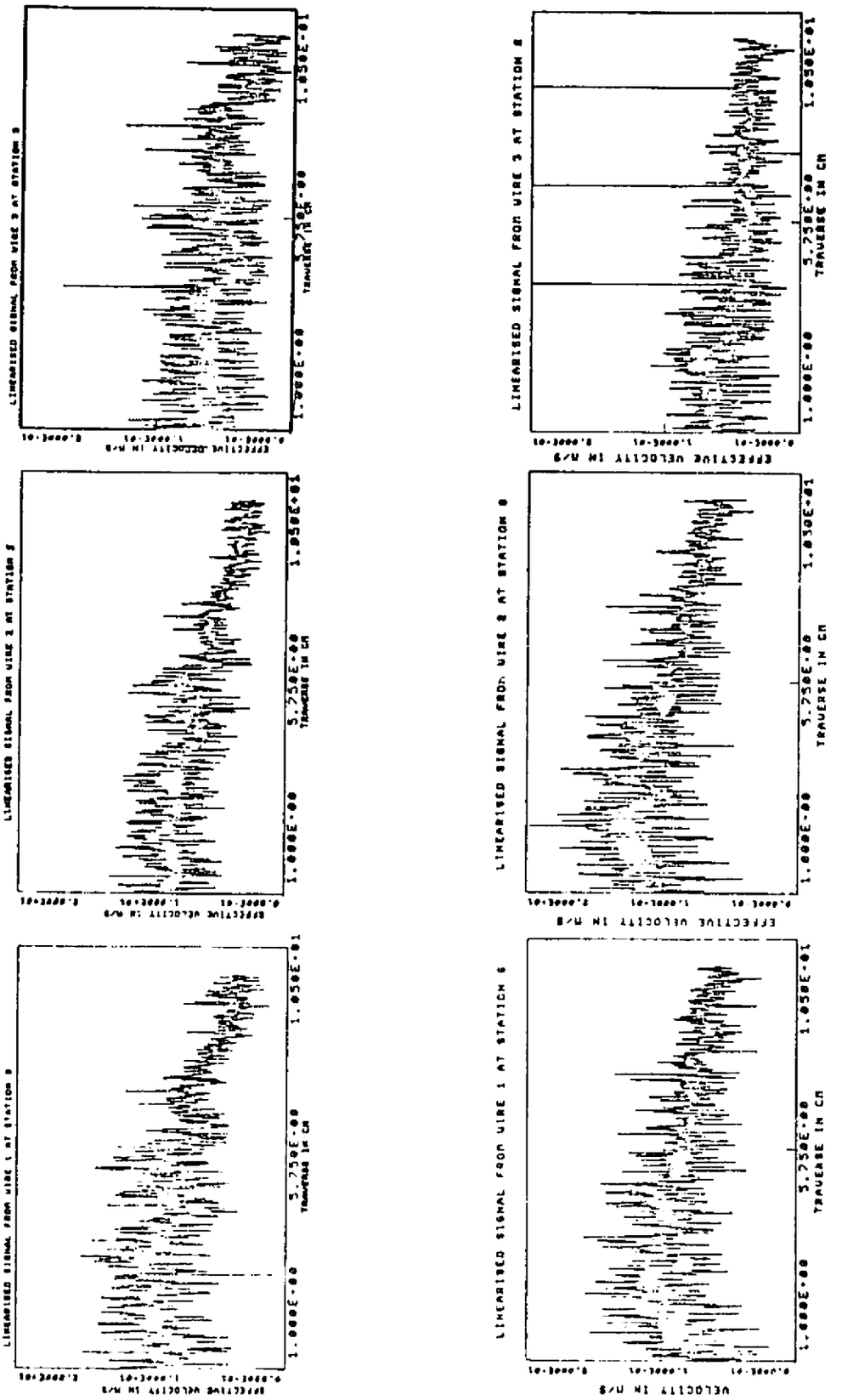
LINEARISED SIGNAL FROM WIRE 3 AT STATION 8
LINEARISED SIGNAL FROM WIRE 2 AT STATION 8
LINEARISED SIGNAL FROM WIRE 1 AT STATION 8
EFFECTIVE VELOCITY IN M/S
TRAVERSE IN CM
1.000E-00
5.250E-00
1.050E-01

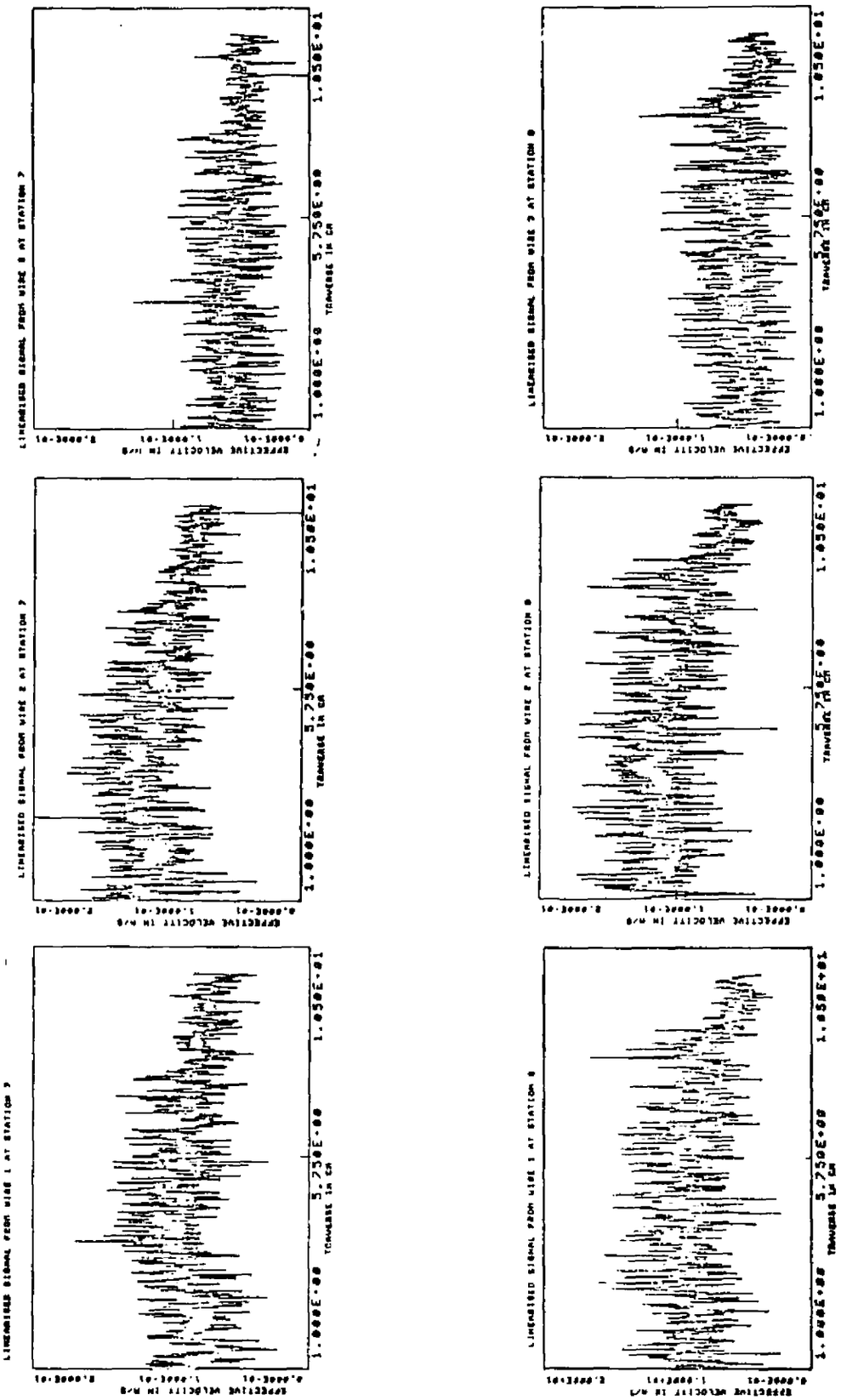

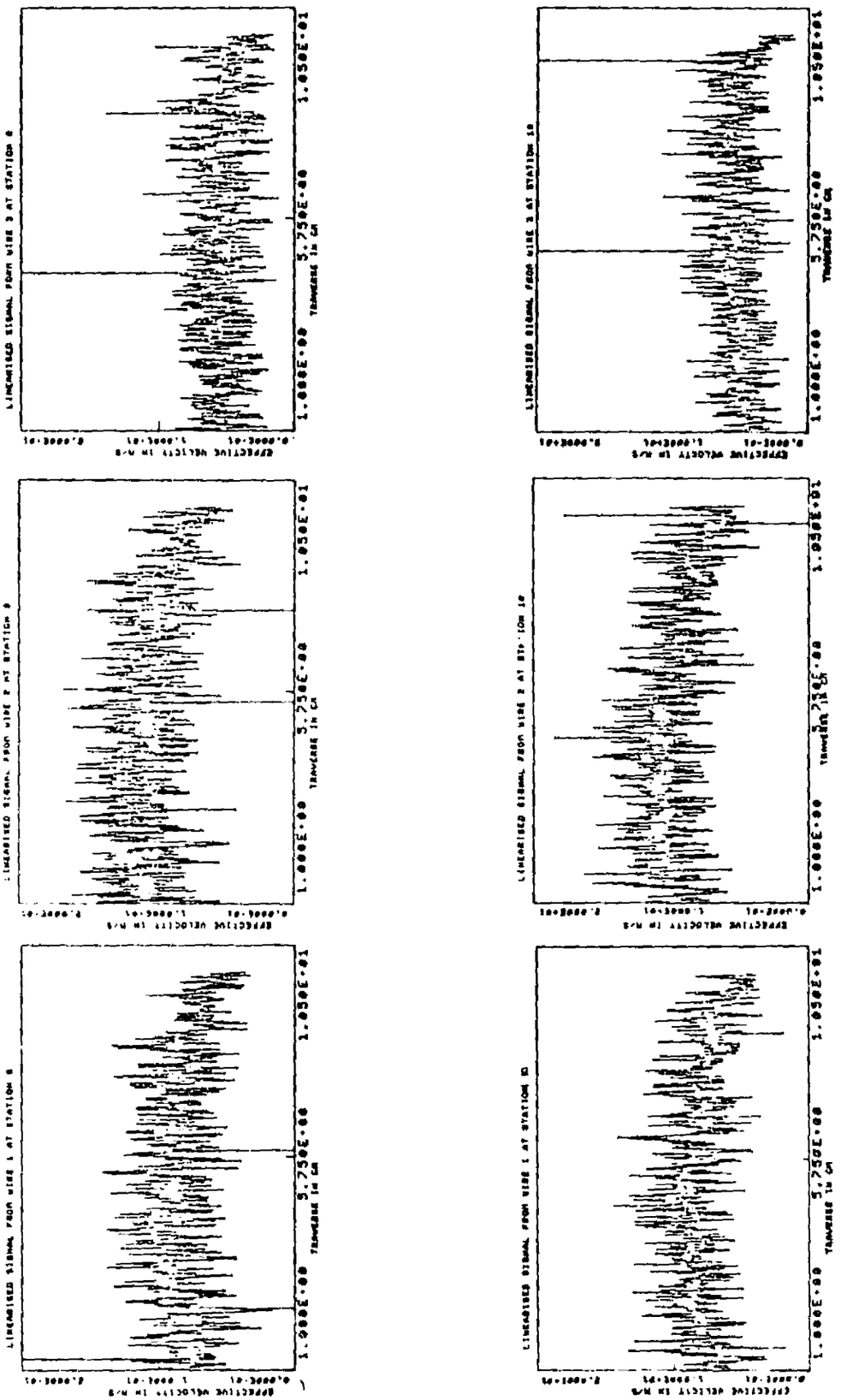

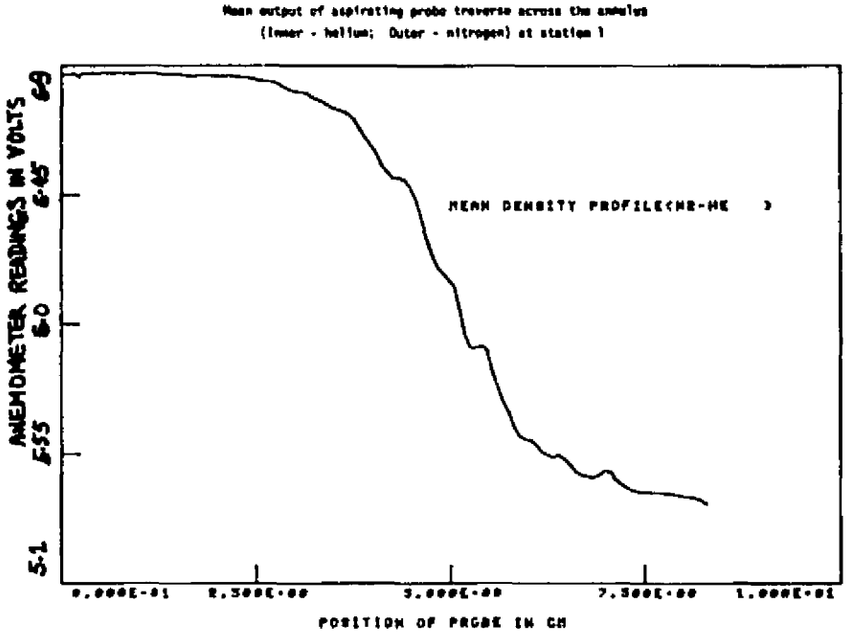
Mean output of aspirating probe traverse across the annulus
(Inner - helium; Outer - nitrogen) at station 1
ANEMOMETER READINGS IN VOLTS
6.9
6.45
6.0
5.55
5.1
MEAN DENSITY PROFILE(HE-HE)
0.000E-01
2.500E+00
5.000E+00
7.500E+00
1.000E+01
POSITION OF PROBE IN CM

Fig. 8a

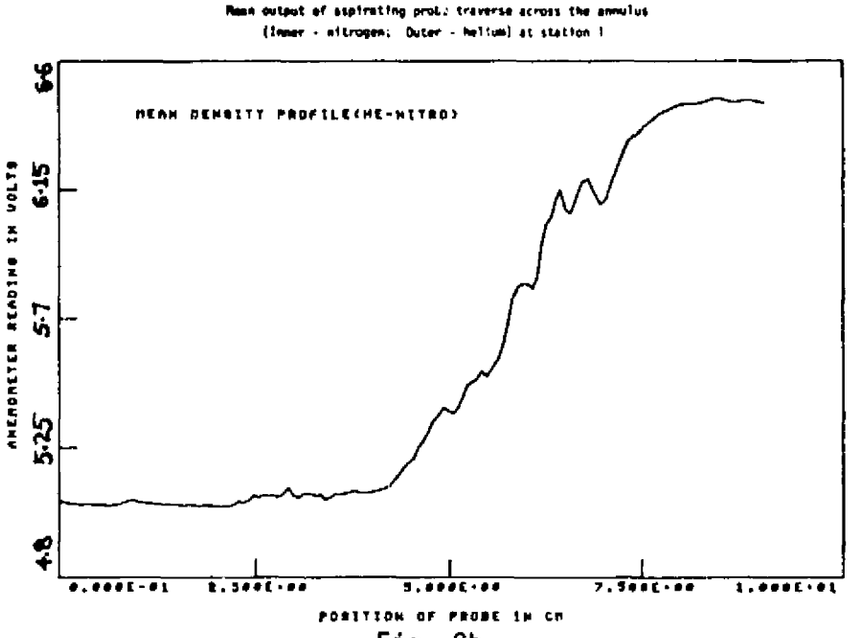
Mean output of aspirating prob. traverse across the annulus
(Inner - nitrogen; Outer - helium) at station 1
ANEMOMETER READING IN VOLTS
6.6
6.15
5.7
5.25
4.8
MEAN DENSITY PROFILE(HE-NITRO)
0.000E-01
2.500E+00
5.000E+00
7.500E+00
1.000E+01
POSITION OF PROBE IN CM

Fig. 8b

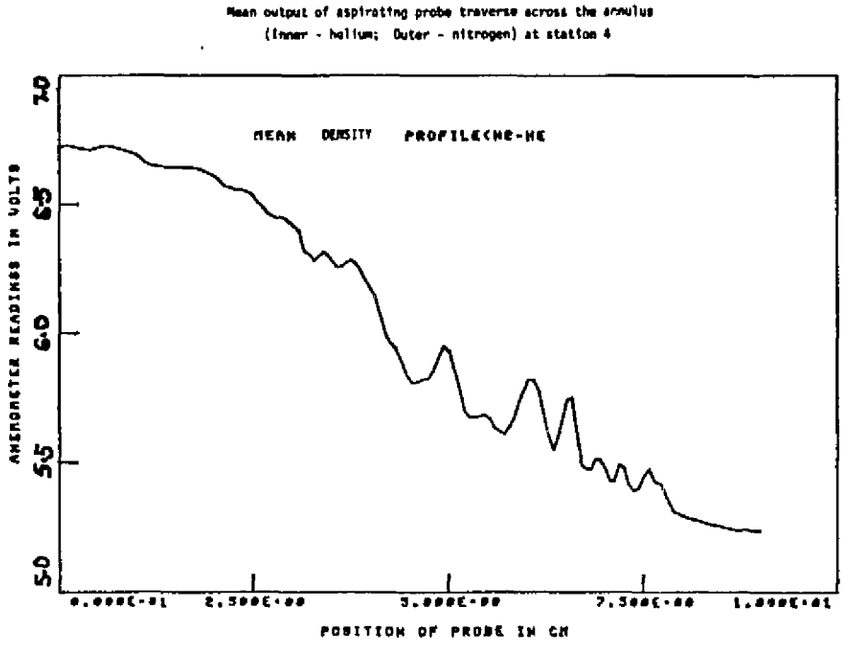
Mean output of aspirating probe traverse across the annulus
(Inner - helium; Outer - nitrogen) at station 4
MEAN DENSITY PROFILE(HE-HE
ANEMOMETER READINGS IN VOLTS
7.0
6.5
6.0
5.5
5.0
POSITION OF PROBE IN CM

Fig. 9a

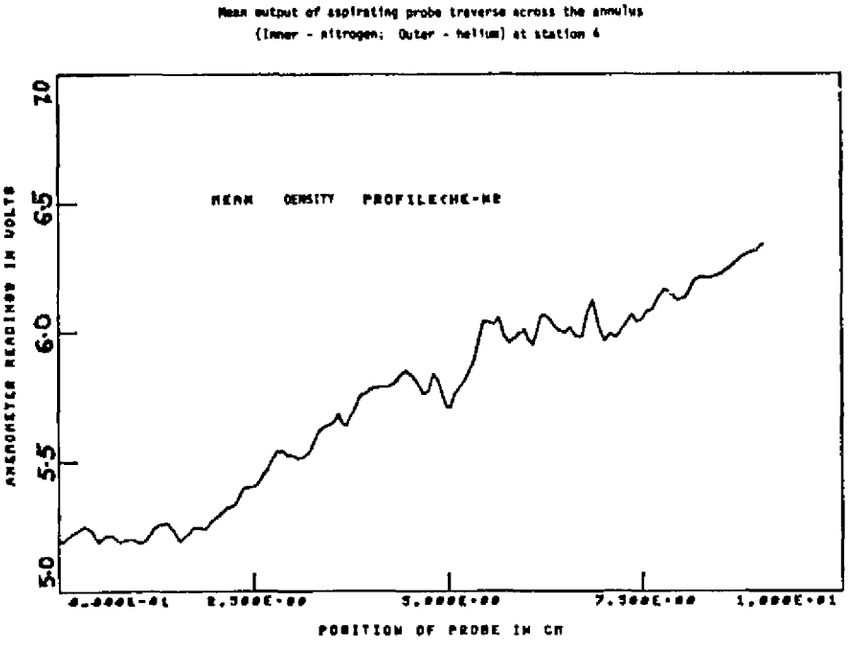
Mean output of aspirating probe traverse across the annulus
(Inner - nitrogen; Outer - helium) at station 4
MEAN DENSITY PROFILE(HE-HE
ANEMOMETER READINGS IN VOLTS
7.0
6.5
6.0
5.5
5.0
POSITION OF PROBE IN CM

Fig. 9b

The pictures are blown-up view of the originals using Polaroid type #52 film.

Notation:

The letter following the picture number (e.g., #1a) refers to flow visualisation picture taken at the same location with the flash-tube fired at a different time after the flow is steady for the blown-down period.

The number in seconds is the time at which the flash-tube is fired.

The number in inches is the distance the center of the picture is from the splitting cylinder.

Fig. 10: Direct excitation pictures (as viewed from side window) for co-flowing streams of equal density with the inner stream set to swirl.

Direction of flow is from right to left.

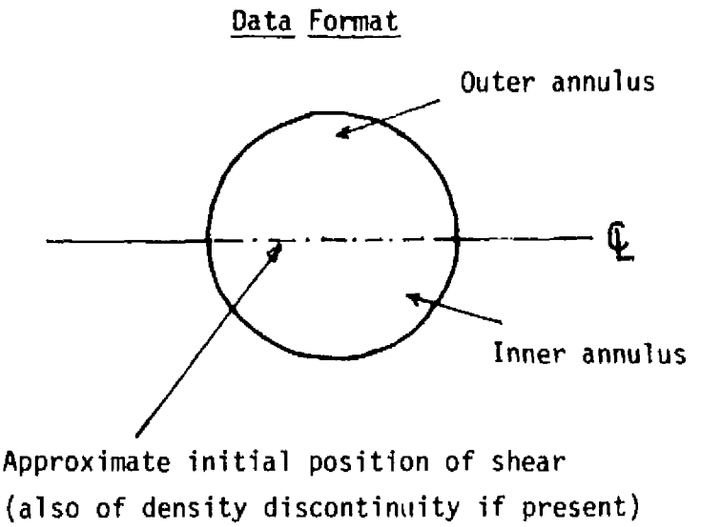

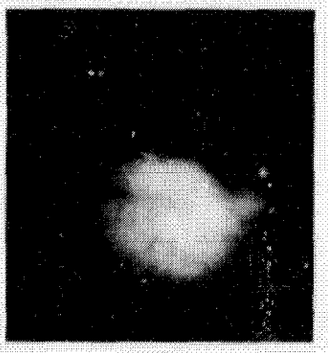

#1 a

3 5/8"

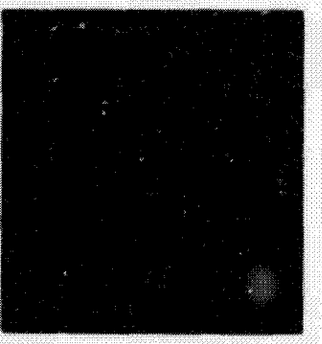

#2 c

5 7/8"

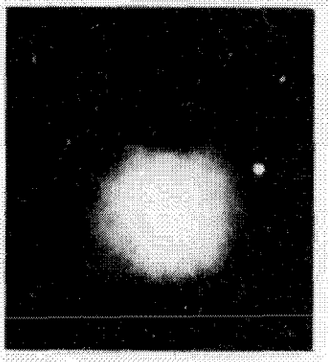

#1 b

3 5/8"

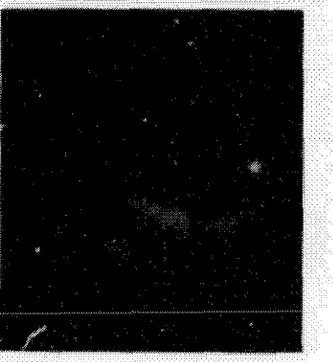

#3 a

1.5 sec

7 3/8"

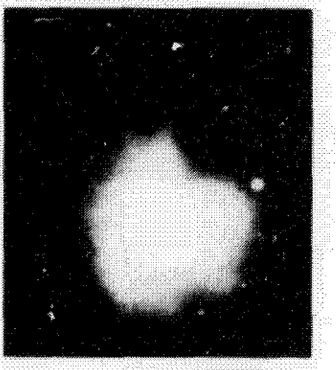

#2 a

5 7/8"

#3 b

1.65 sec

7 3/8"

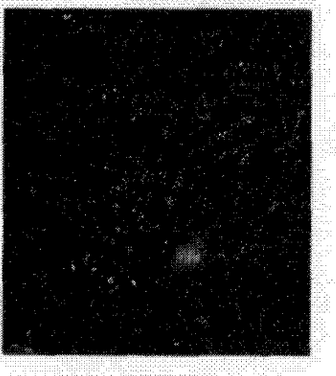

#2 b

5 7/8"

#3 c

1.7 sec

7 3/8"

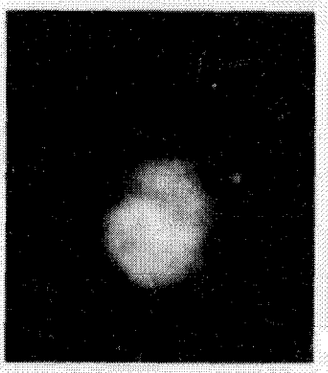

#4 a

1.65 sec

10 3/8"

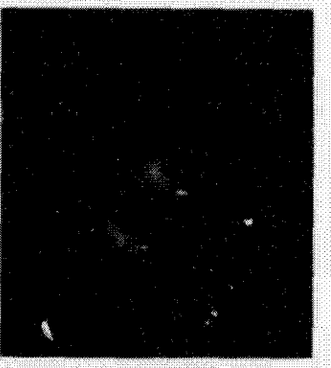

#6 a

1.6 sec

14 3/8"

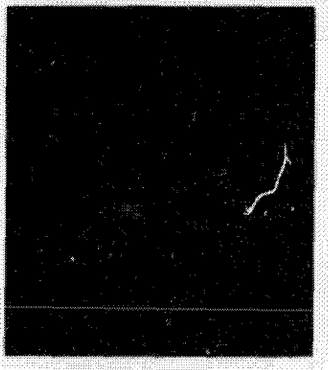

#4 b

1.8 sec

10 3/8"

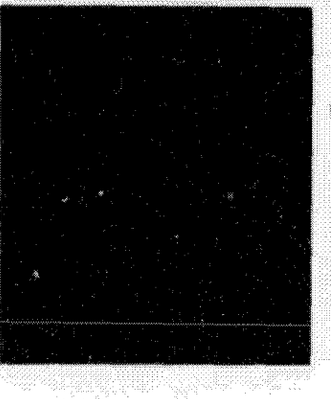

#6 b

1.8 sec

14 3/8"

#5 a

1.65 sec

12 7/8"

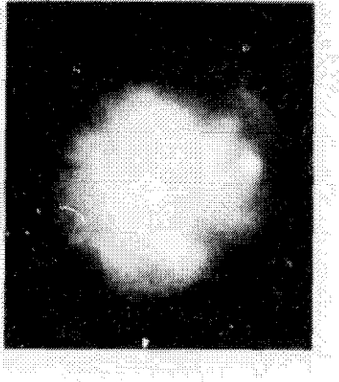

#5 b

1.8 sec

12 7/8"

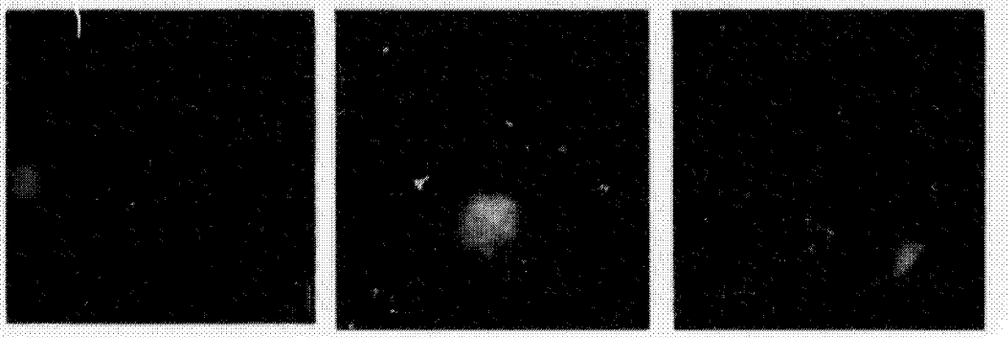

1 # 2 # 3

$3\frac{5"}{8}$ $5\frac{7"}{8}$ $7\frac{3"}{8}$

Fig. 11: Quenching pictures (as viewed from side window) for co-flowing streams of equal density with the inner stream set to swirl.

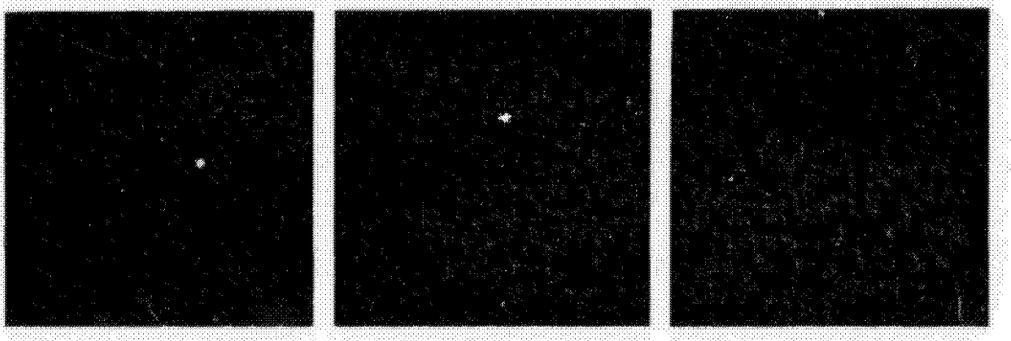

1 # 2 # 3

$3\frac{5"}{8}$ $5\frac{7"}{8}$ $10\frac{3"}{8}$

Fig. 12: Collisional excitation pictures (as viewed from side window) for co-flowing streams of equal density with the inner stream set to swirl.

Fig. 13: Direct excitation pictures of flow field in axial plane (as viewed from an axial direction) for co-flowing streams of equal density with the inner stream set to swirl.

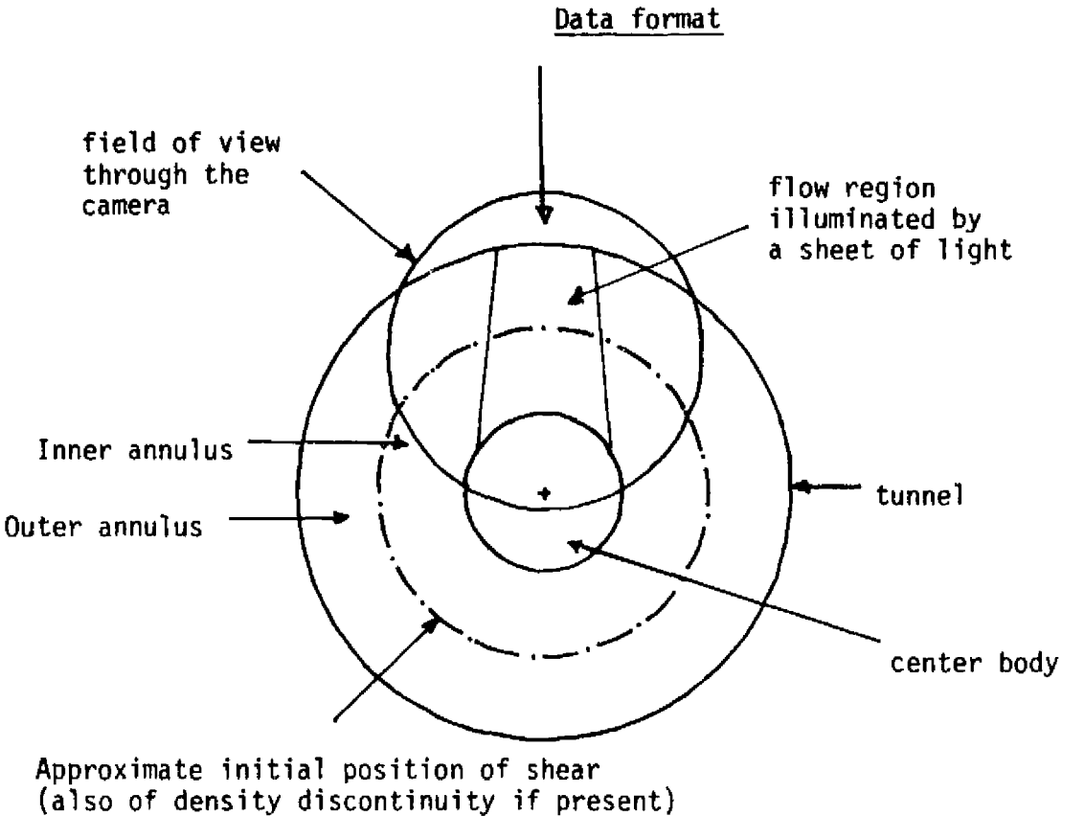

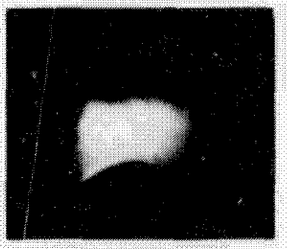

1

2 1/2"

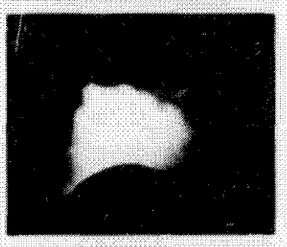

2

3 1/2"

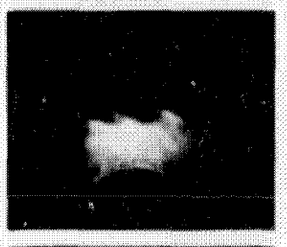

3

4 1/2"

4

5"

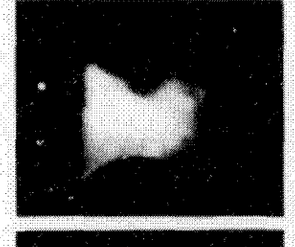

5

5 1/2"

6

6"

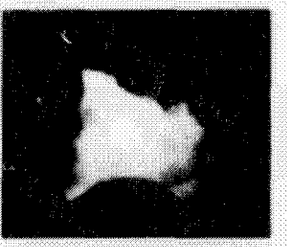

7

6 1/2"

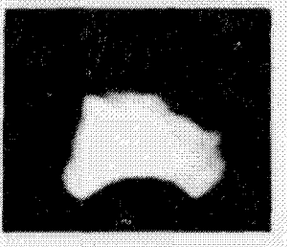

8

7"

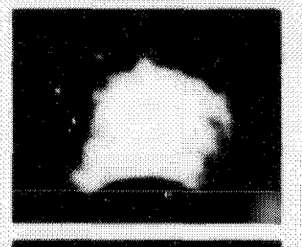

9

7 1/2"

10 a

1.6 sec

9 1/2"

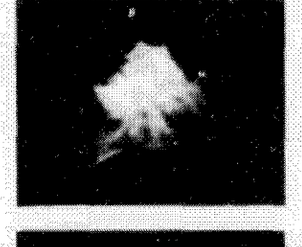

10 b

1.7 sec

9 1/2"

10 c

1.85 sec

9 1/2"

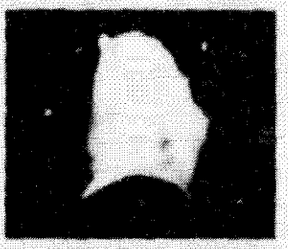

11 a
1.65 sec
10"

11 b
1.8 sec
10"

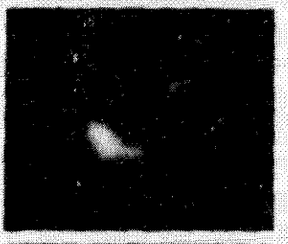

12 a
1.6 sec
10 1/2"

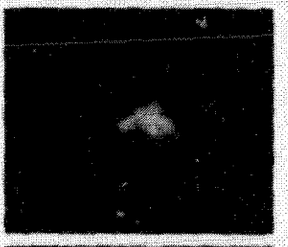

12 b
1.7 sec
10 1/2"

12 c
1.85 sec
10 1/2"

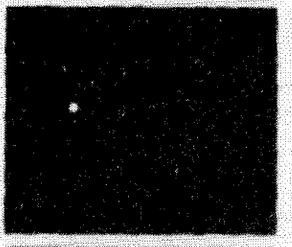

13 a
1.6 sec
11 1/2"

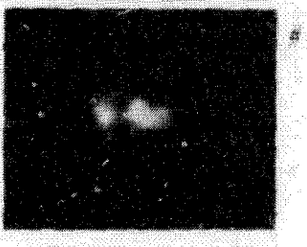

13 b
1.7 sec
11 1/2"

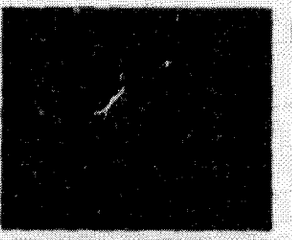

13 c
1.85 sec
11 1/2"

14 a
1.6 sec
12"

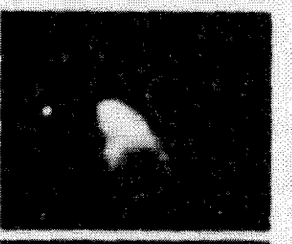

14 b
1.7 sec
12"

14 c
1.85 sec
12"

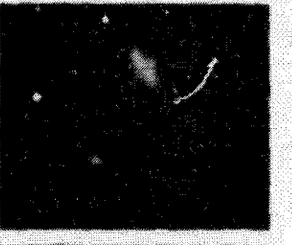

15 a
1.6 sec
12 1/2"

15 b
1.7 sec
12 1/2"

15 c
1.85 sec
12 1/2"

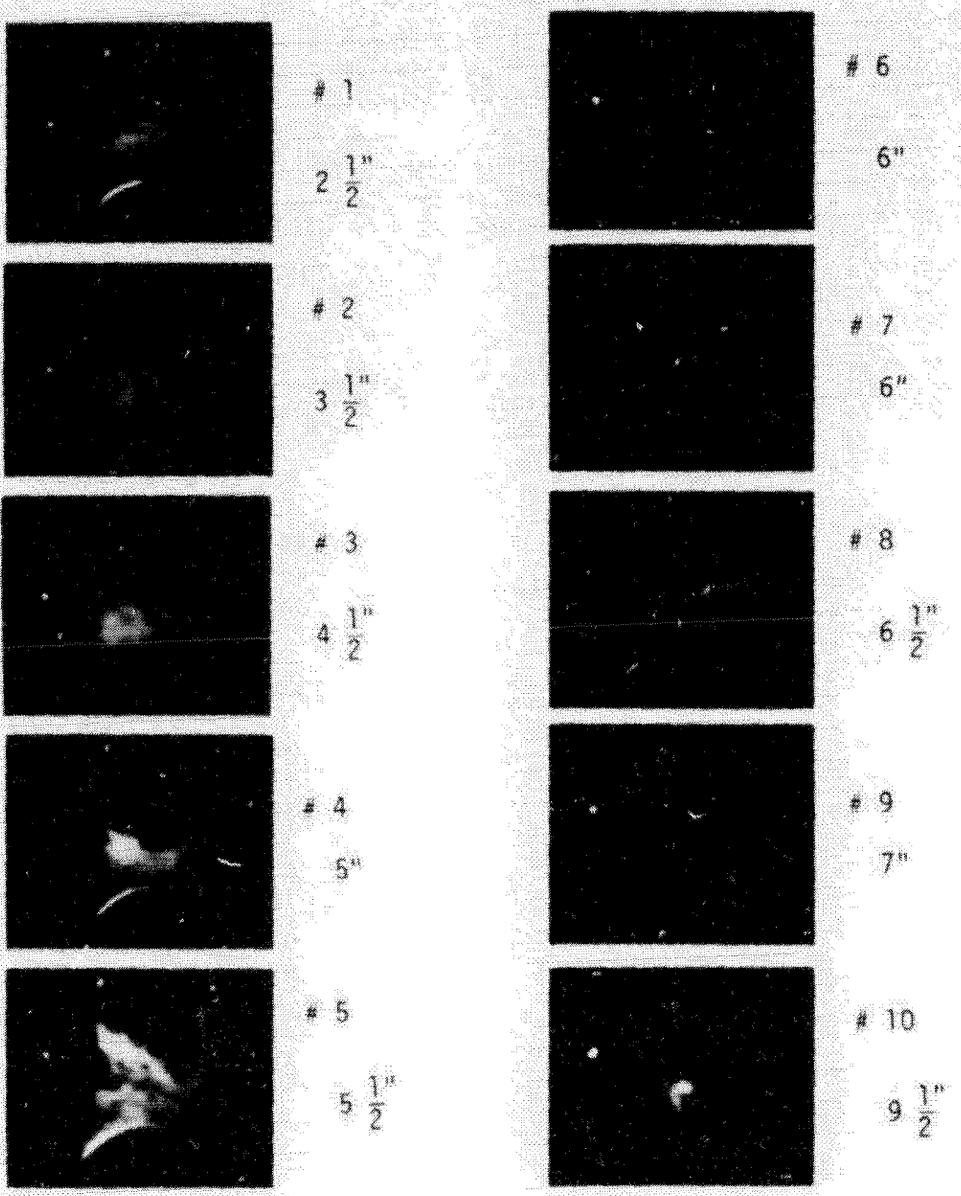

Fig. 14: Quenching pictures (as viewed from the axial direction) for co-flowing streams of equal density with the inner stream set to swirl.

1

9 1/2"

Fig. 15: Collisional excitation picture for flow field in axial plane (as viewed from the axial direction) for co-flowing streams of equal density with inner stream set to swirl

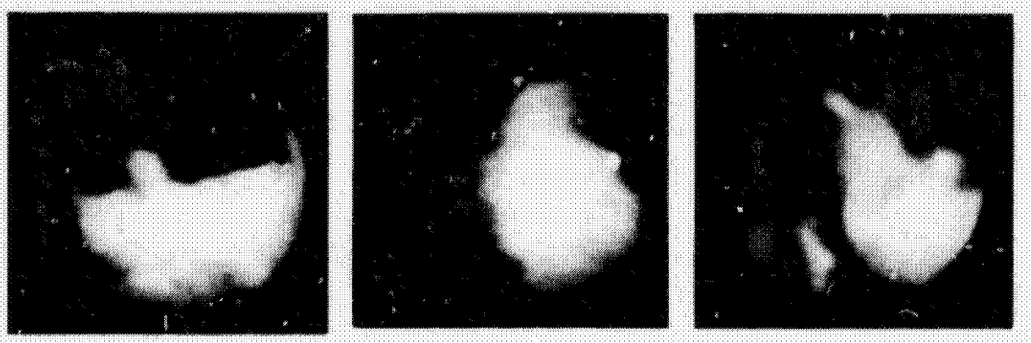

1 # 2 # 3

$3\frac{5"}{8}$ $5\frac{7"}{8}$ $7\frac{3"}{8}$

Fig. 16: Direct excitation pictures (as viewed from side window) for co-flowing streams of different densities (inner- nitrogen, outer - helium) with the inner stream set to swirl.

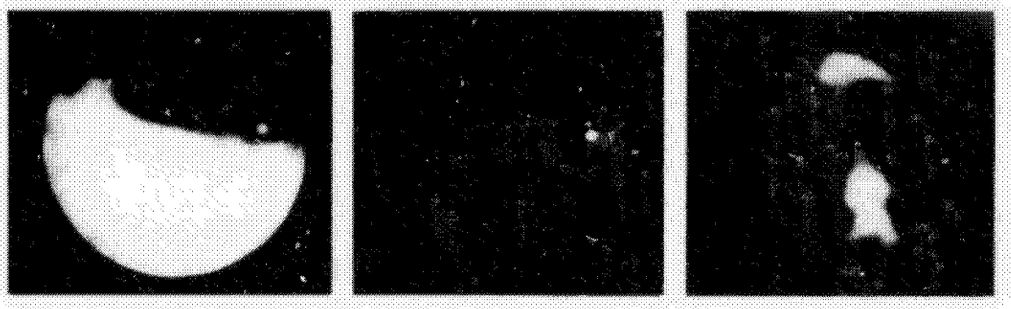

1 # 2 # 3

$3\frac{5"}{8}$ $5\frac{7"}{8}$ $7\frac{3"}{8}$

Fig. 17: Quenching pictures (as viewed from side window) for co-flowing streams of different densities (inner - nitrogen, outer - helium) with the inner stream set to swirl

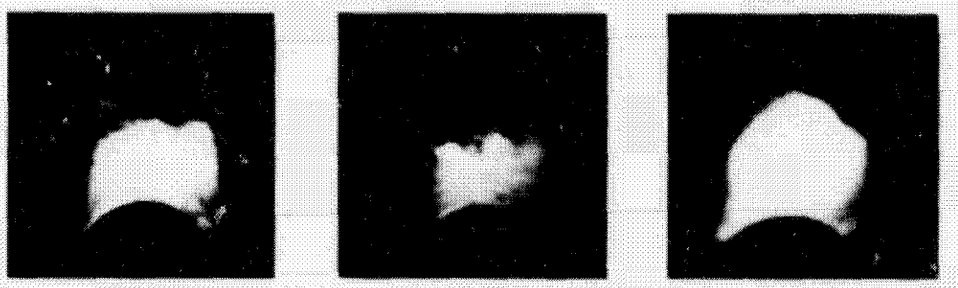

1 # 2 # 3

$2\frac{1}{2}$" $3\frac{1}{2}$" 5"

Fig. 18: Direct excitation pictures (as viewed from axial direction) for co-flowing streams of different density (inner - nitrogen, outer - helium) with inner stream set to swirl.

1 # 2 # 3

$2\frac{1}{2}$" $3\frac{1}{2}$" 5"

Fig. 19: Quenching pictures (as viewed from the axial direction) for co-flowing steams of different densities (inner-nitrogen, outer - helium) with the inner stream set to swirl.

1 # 2 # 3

$3\frac{5''}{8}$ $5\frac{7''}{8}$ $7\frac{3''}{8}$

Fig. 20: Direct excitation pictures (as viewed from side window) for co-flowing streams of different densities (inner - helium, outer - nitrogen) with the inner stream set to swirl.

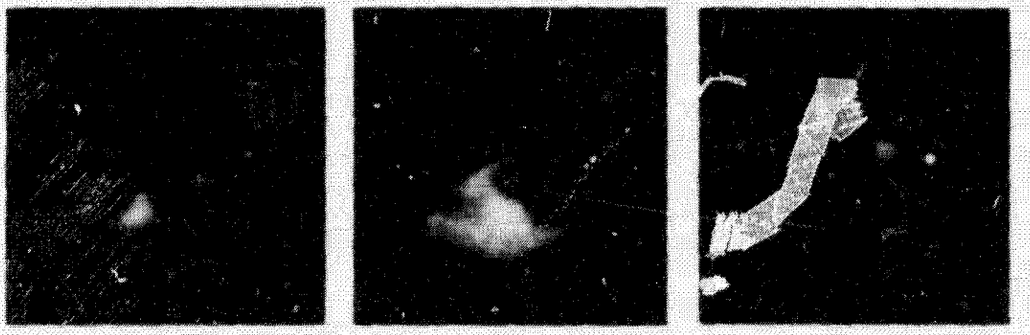

1 # 2 # 3

$3\frac{5''}{8}$ $5\frac{7''}{8}$ $7\frac{3''}{8}$

Fig. 21: Quenching pictures (as viewed from side window) for co-flowing streams of different densities (inner - helium, outer - nitrogen) with the inner stream set to swirl.

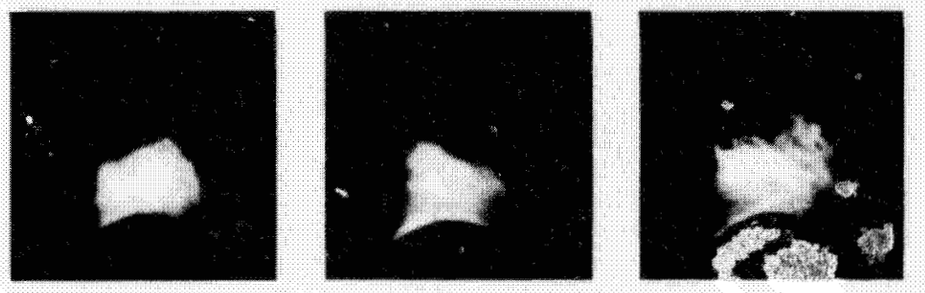

1 # 2 # 3

$2\frac{1}{2}$" $3\frac{1}{2}$" 5"

Fig. 22: Direct excitation pictures (as viewed from the axial direction) for co-flowing streams of different densities (inner - helium, outer - nitrogen) with the inner stream set to swirl.

1 # 2 # 3

$2\frac{1}{2}$" $3\frac{1}{2}$" 5"

Fig. 23: Quenching pictures (as viewed from the axial direction) for co-flowing streams of different densities (inner - helium, outer - nitrogen) with the inner stream set to swirl.

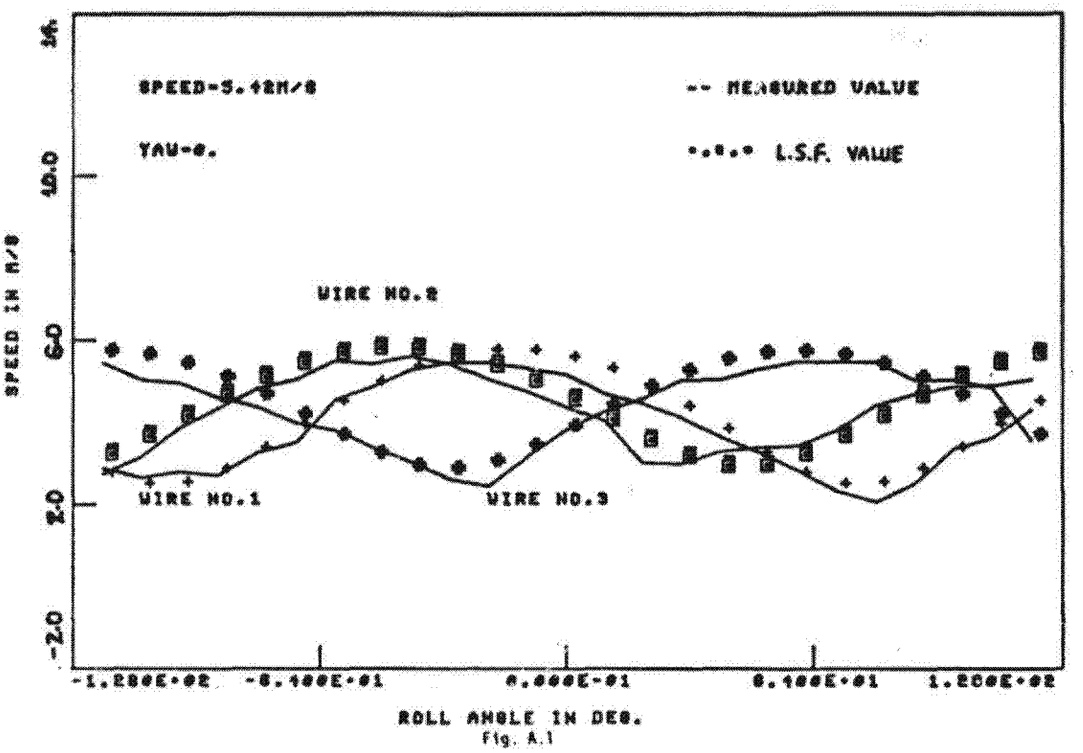
SPEED=5.42M/S
YAW=0.
-- MEASURED VALUE
..* L.S.F. VALUE
WIRE NO.2
WIRE NO.1
WIRE NO.3
SPEED IN M/S
10.0
6.0
2.0
-2.0
-1.280E+02
-6.400E+01
0.000E+01
6.400E+01
1.280E+02
ROLL ANGLE IN DEG.

Fig. A.1

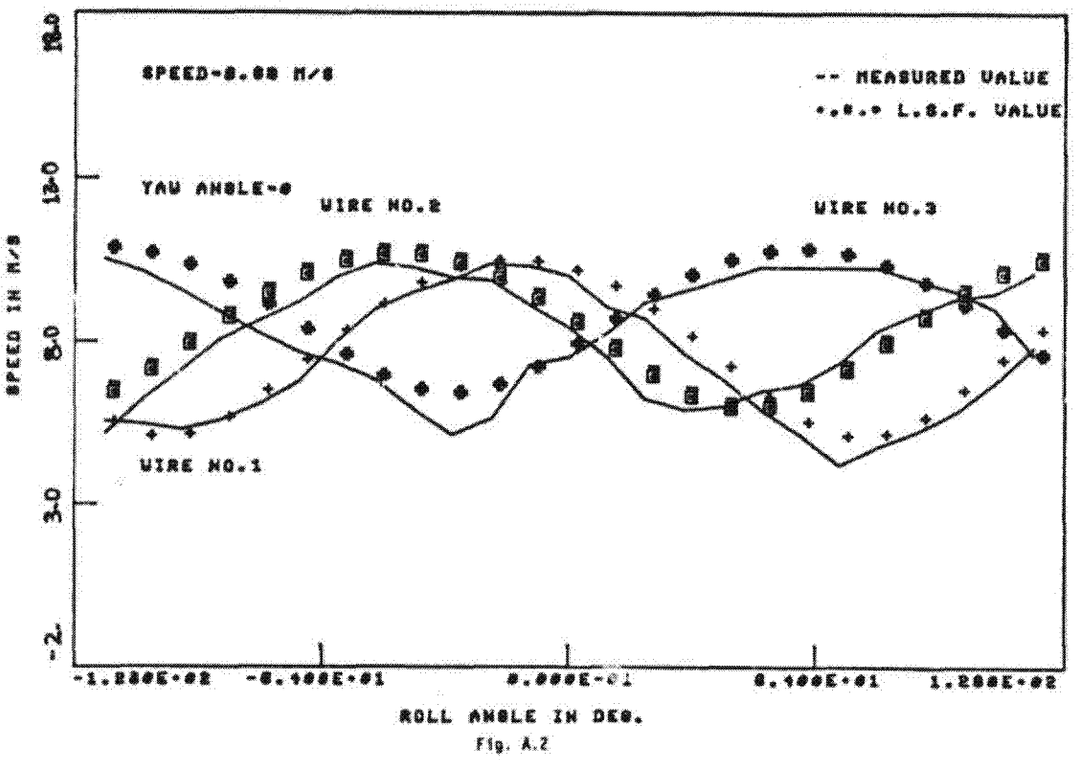
SPEED=8.88 M/S
YAW ANGLE=0
-- MEASURED VALUE
..* L.S.F. VALUE
WIRE NO.2
WIRE NO.3
WIRE NO.1
SPEED IN M/S
13.0
8.0
3.0
-2.
-1.280E+02
-6.400E+01
0.000E+01
6.400E+01
1.280E+02
ROLL ANGLE IN DEG.

Fig. A.2

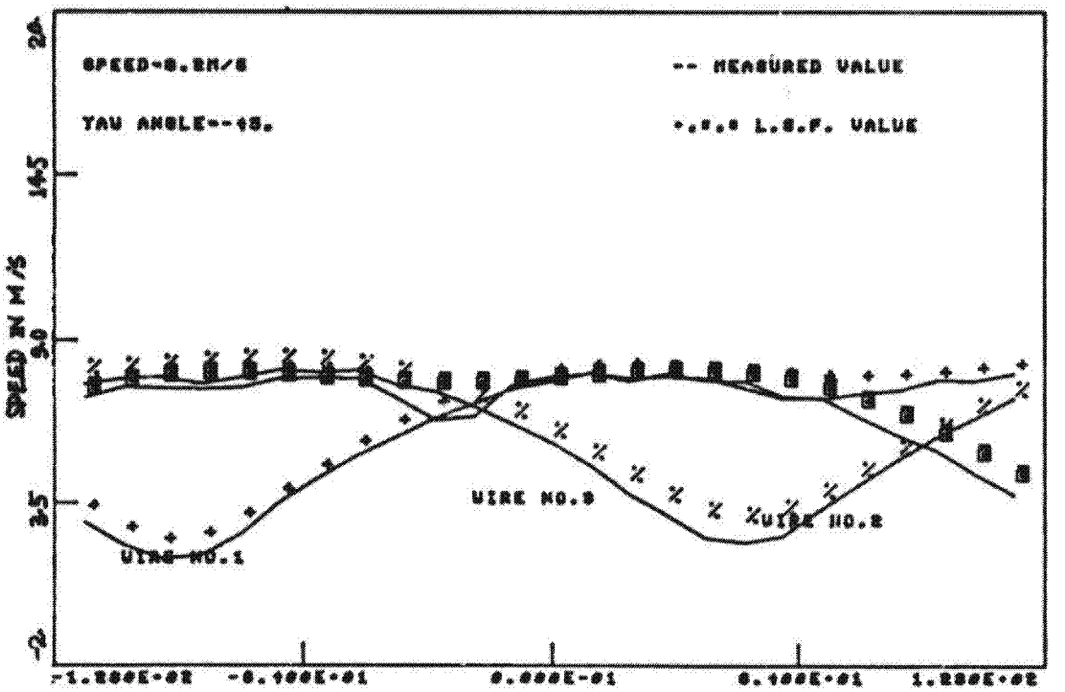
SPEED=8.8M/S
YAW ANGLE=-15.
-- MEASURED VALUE
•.•.• L.S.F. VALUE
SPEED IN M/S
WIRE NO.3
WIRE NO.1
WIRE NO.2
ROLL ANGLE IN DEG.

Fig. A.3

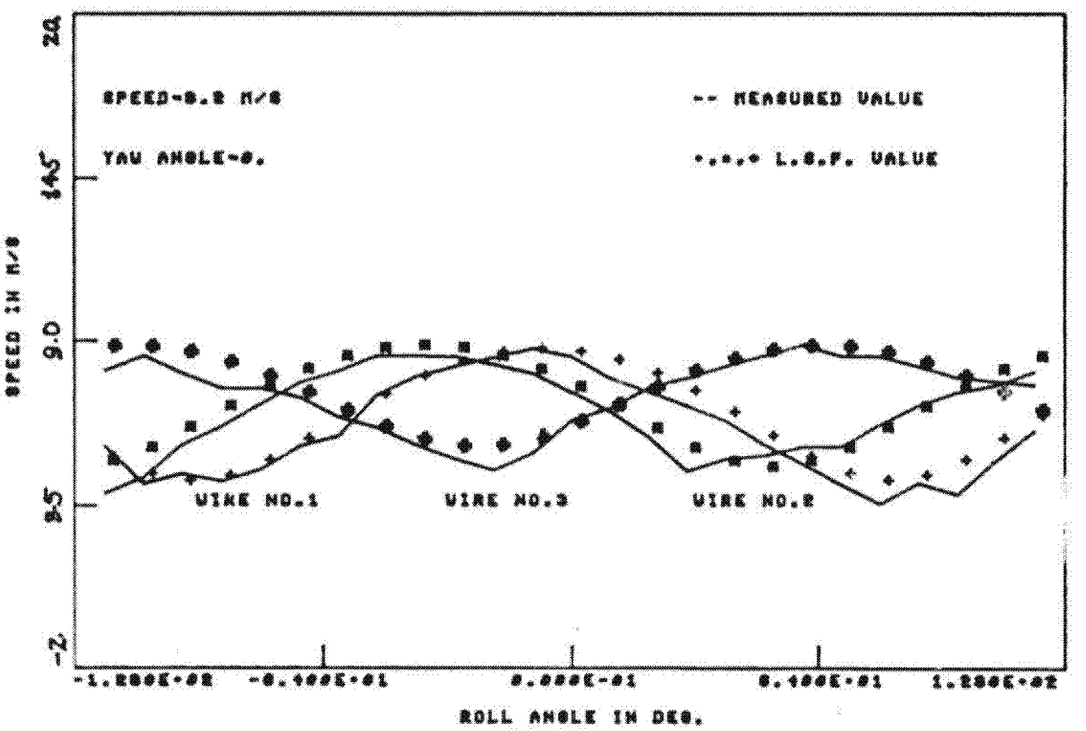
SPEED=8.8 M/S
YAW ANGLE=0.
-- MEASURED VALUE
•.•.• L.S.F. VALUE
SPEED IN M/S
WIRE NO.1
WIRE NO.3
WIRE NO.2
ROLL ANGLE IN DEG.

Fig. A.4

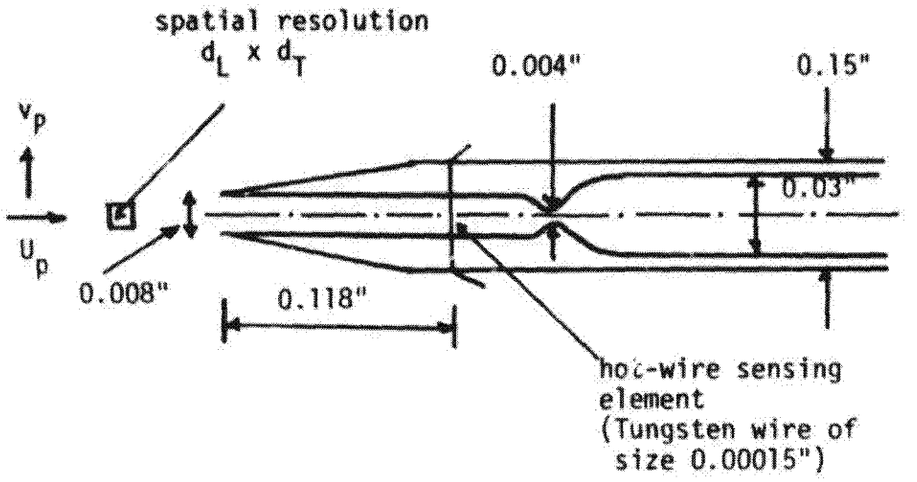

Fig. B.1: Aspirating Probe

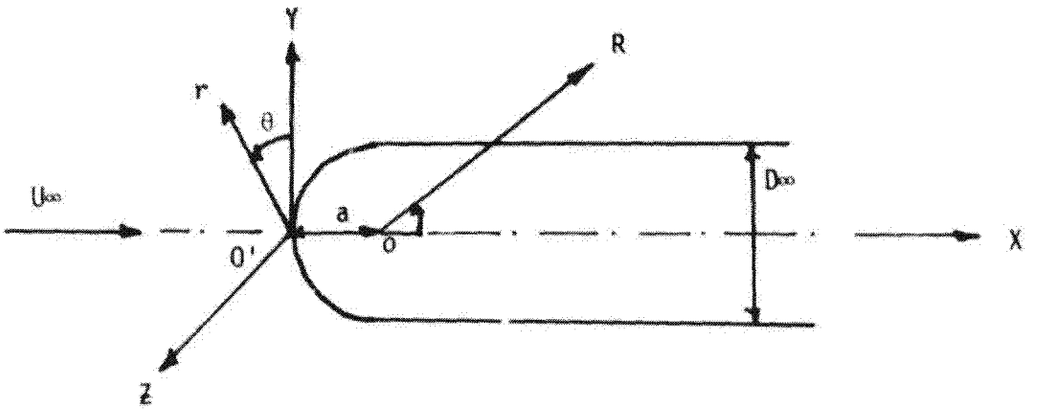

Fig. B.2

suction rate = 1.59×10^{-6} m^3/s

free stream velocity = $7\ ms^{-1}$

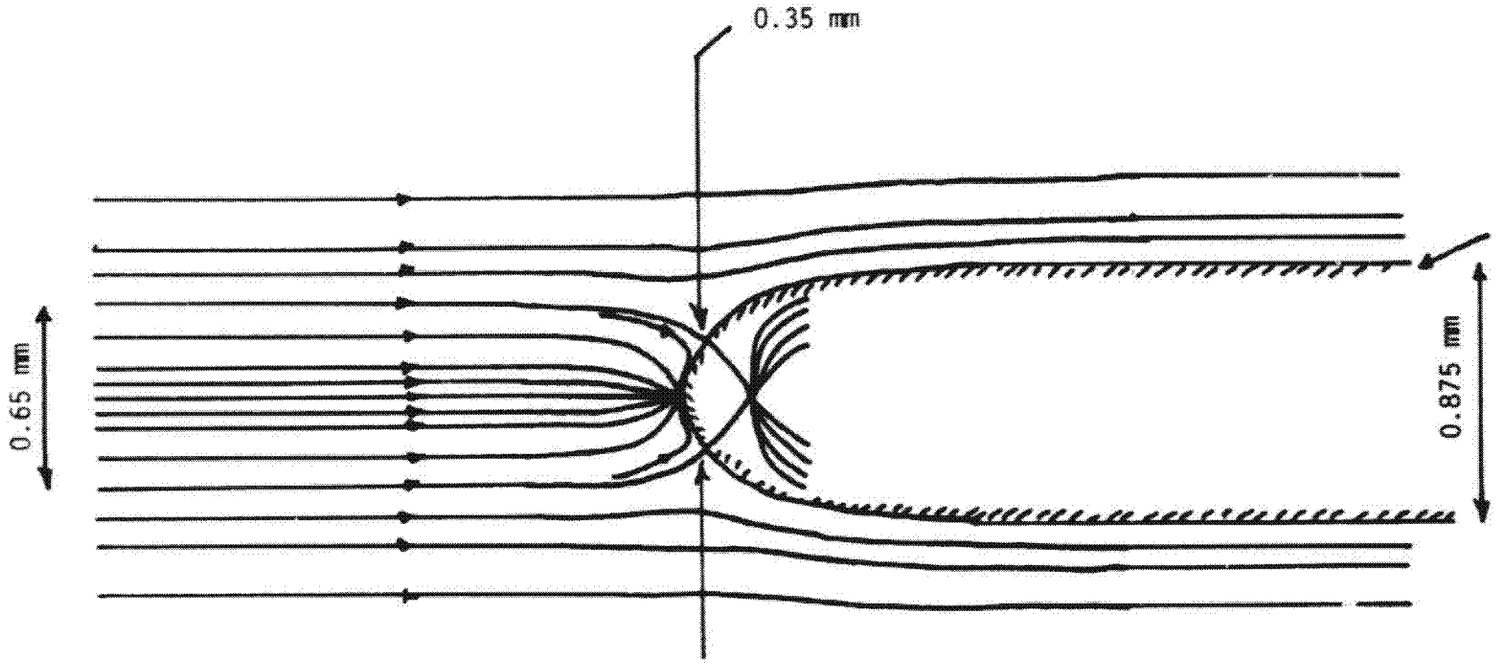

Fig. 5.3: Flow around an axisymmetric Rankine-type body with a weak sink placed at its tip.

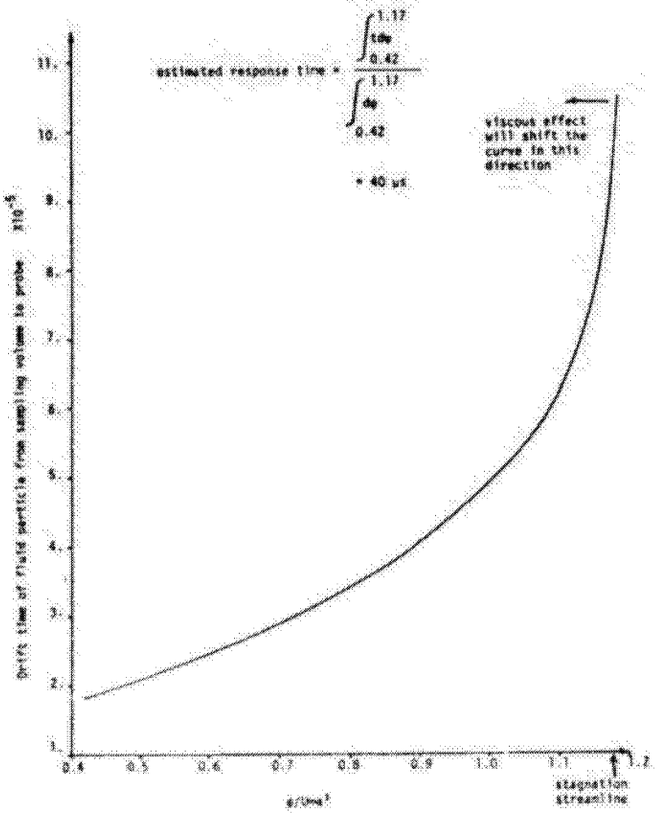

Fig. B.4

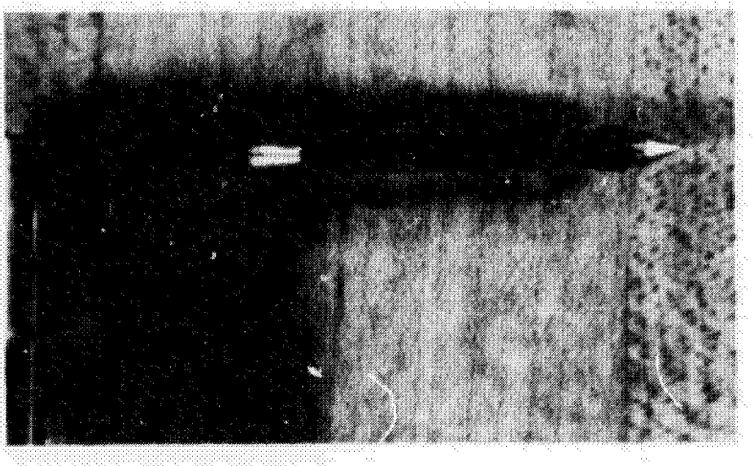

Fig. B.5 Aspirating probe

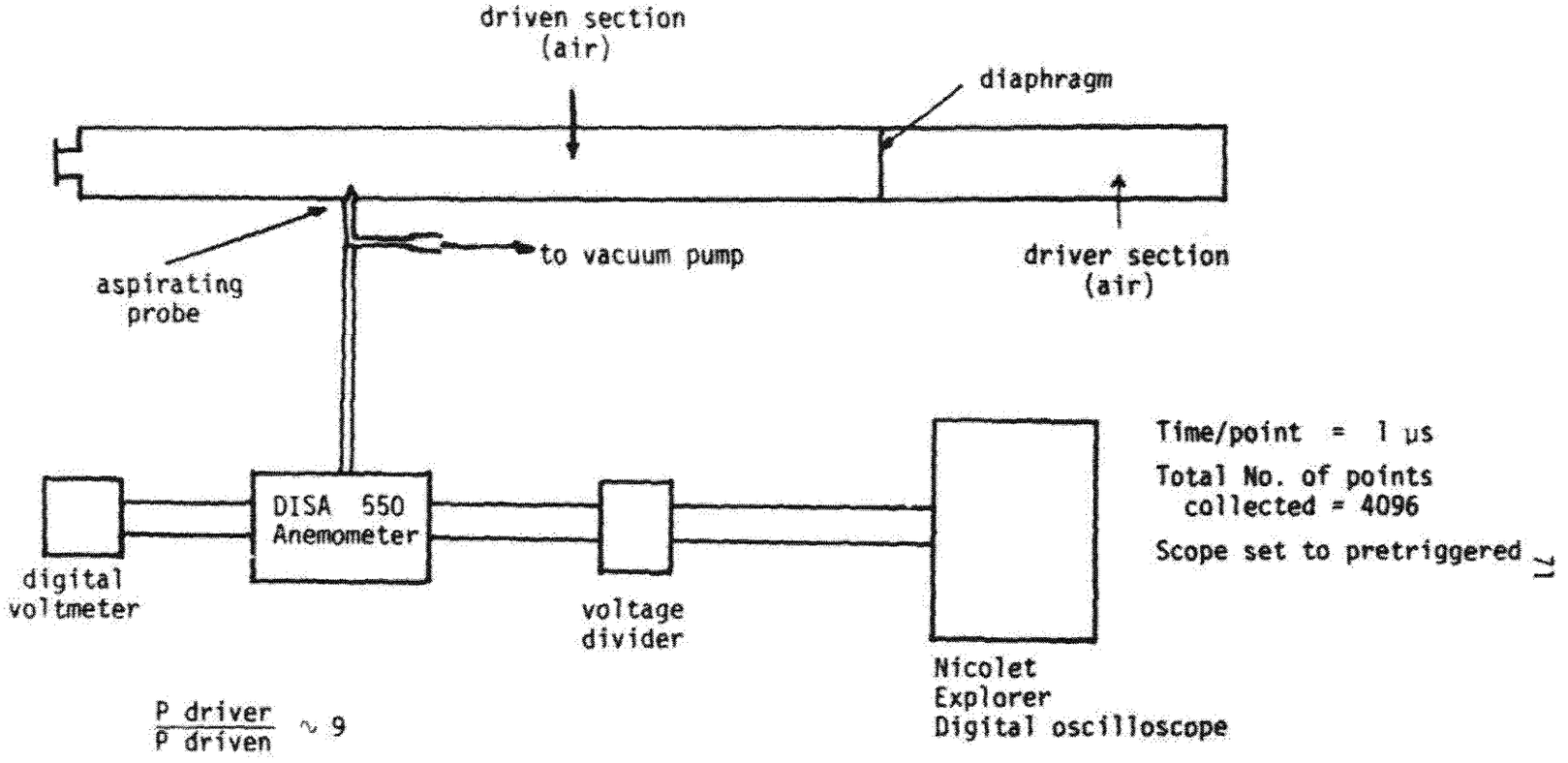

(contraction in area at end of shock tube will cause reflection of shock wave)

Fig. B.6 Set-up to measure probe response time

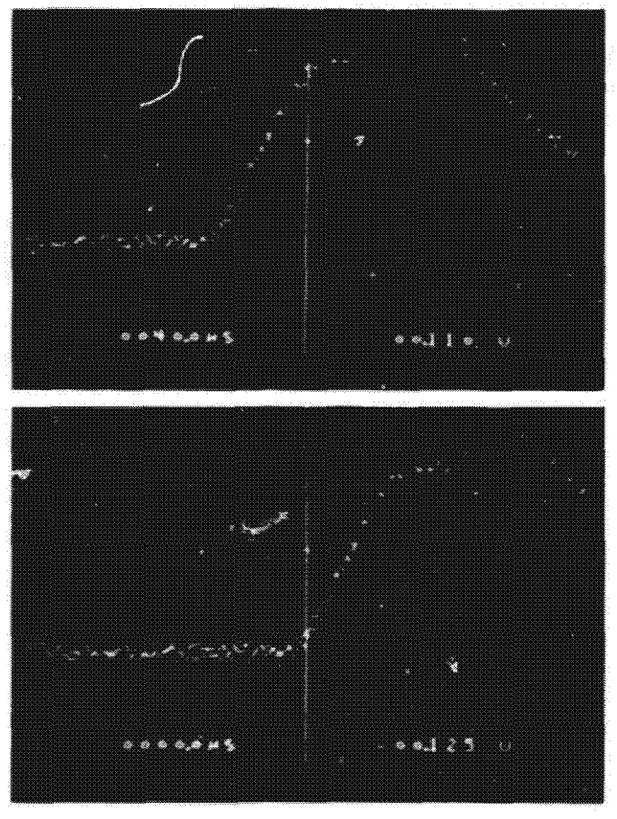

Fig. B.7a: Output of Digital Oscilloscope: response time of probe = 40 μs

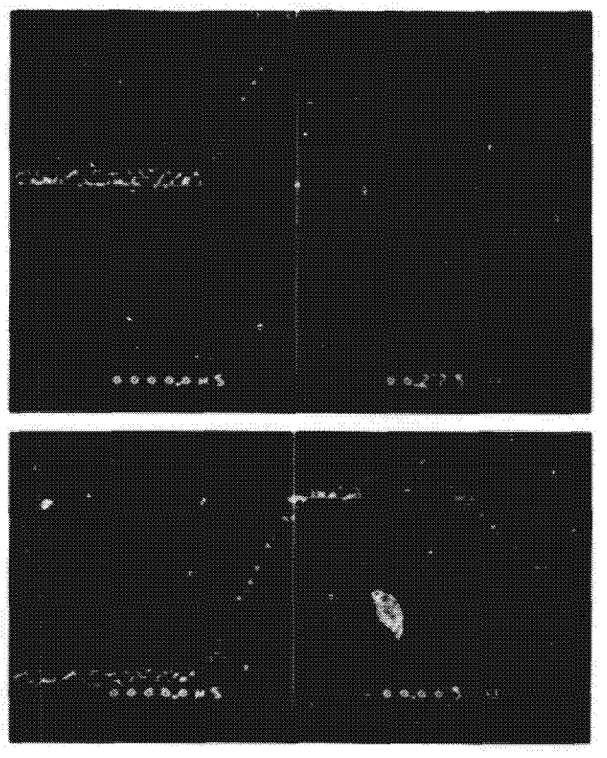

Fig. B.7b: Output of digital scope: amplitude of response = 0.28v